Published in: *Phys Chem Chem Phys.* 2011 October 21; 13(39): 17484–17493. doi:10.1039/c1cp20520j

J-Coupling Constants for a Trialanine Peptide as a function of Dihedral Angles Calculated by Density Functional Theory over the full Ramachandran Space

Pedro Salvador[‡,*], **I-Hsien (Midas) Tsai**, and **J. J. Dannenberg**[‡‡,*]
Department of Chemistry, City University of New York - Hunter College and the Graduate School, 695 Park Avenue, New York NY 10065; Institute of Computational Chemistry and Department of Chemistry, University of Girona, 17071 Girona (Catalonia)

Abstract

We present 13 ^{3}J, seven ^{2}J and four ^{1}J coupling constants (24 in all) calculated using B3LYP/D95** as a function of the ϕ and ψ Ramachandran dihedral angles of the acetyl(Ala)$_3$NH$_2$ capped trialanine peptide over the entire Ramachandran space. With the exception of three of these J couplings, all show significant dependence upon both dihedral angles. For each J coupling considered, a two dimensional grid with respect to ϕ and ψ angles can be used to interpolate the values for any pair of ϕ and ψ values. Such simple interpolation is shown to be very accurate. Most of these calculated J couplings should prove useful for improving the accuracy of the determination of peptide and protein structure from NMR measurements in solution over that provided by the common procedure of treating the J couplings as functions of a single dihedral angle by means of Karplus-type fittings.

Chemists have used ^{3}J coupling constants to determine the structures of molecules since Karplus showed that vicinal ^{3}J(H,H') couplings are a function of HCCH' dihedral angles.[1] Individual dihedral angular relationships for peptide and protein backbones have been determined using correlations of experimental J's with crystallographic data.[2–4] Structural protein chemists have extended these relationships and combined them with others to determine the structures of proteins and peptides in solution.[4–15] Recently, we published a DFT study of the energies of acetyl(Ala)$_3$NH$_2$ as a function of the torsional angles about the central Ala residue in the manner of Ramachandran.[16] Since we have optimized 5184 individual structures at different sets of fixed ψ's and ϕ's, we thought it useful to calculate all possible J-coupling constants for these conformations. Six ^{3}J's can be determined for rotation about each of the two dihedral angles, yielding 12 total. In addition the ^{3}J between C_{13} and H_{22} (see figure 1 for notation) whose formal dihedral is about the peptide bond has been found to vary with the ψ angle is included in this study. Two ^{1}J's and six ^{2}J's can also be calculated from the conformational data using only the ϕ and ψ dihedrals.

Previous studies have generally only considered the dihedral about the C-N bond (ϕ) without taking into account the influence of rotation about the C-C bond (ψ) upon the J's, although Kozminski, et al. considered both dihedrals in a study of ^{2}J($C_{13}N_{21}$)'s. These studies mostly lead to Karplus-like equations that relate the J's to a single dihedral angle. In this paper we evaluate the effect of the second dihedral (C-C) upon the J's predicted by only the first (C-N) and consider the effects of both dihedrals upon the six J's that can be defined around the

*pedro.salvador@udg.edu, jdannenberg@gc.cuny.edu.
‡University of Girona.
‡‡City University of New York, visiting professor University of Girona, 2006..

C-C dihedral. The eventual goal will be to develop a method that uses up to all 12 dihedrals that define the three-bond interactions to determine the local structure of a peptide around a specific residue. We also address the possibility of using also specific ^{1}J and ^{2}J as probes of ψ and ϕ dihedrals for protein structure determination.

Computational Details

All calculations were performed using the same procedures used in our previous work.[17] We used the GAUSSIAN 03[18] and GAUSSIAN 09[19] suites of programs and the B3LYP functional. This method combines Becke's 3-parameter functional,[20] with the non-local correlation provided by the correlation functional of Lee, Yang and Parr.[21] As we previously noted no difference between (unrestricted) UB3LYP and (restricted) B3LYP calculations for several examples, we used B3LYP alone.[22] All calculations used the D95** basis set which we have previously used in other studies of peptide and peptide-like H-bonds. We determined this basis set to be adequate for trans-H-bond ^{13}C-^{15}N ^{h3}J's elsewhere,[22] as it predicted trans-H-bond ^{13}C-^{15}N 3-bond scalar J-couplings that were similar to those predicted by other similar and larger basis sets. In this paper we demonstrate that B3LYP/ D95** provides reasonable results for most J's studied here (see below). The coupling constants were calculated using the 'spin-spin' option in GAUSSIAN 03. This option calculates J's including contributions from the spin-dipole (SD) and both diamagnetic (DSO) and paramagnetic (PSO) spin-orbit terms in addition to the Fermi contact (FC) term.[23–26] As a basis for the present work, we used the geometrical Ramachandran grid of the capped trialanine acetyl-$(Ala)_3$-NH_2 that we optimized for fixed values of the dihedral angles ϕ and ψ of the central alanine residue that we have published elsewhere.[16] These varied in 5 degree intervals in the full range of −180 to 180 degrees of each dihedral (ϕ and ψ), for a total of 5184 optimized structures. In the current work we have used a reduced subset of previously optimized structures, covering the whole Ramachandran space of the central alanine. We have selected 483 of these 5184 geometries at varying intervals of from 10 to 20 degrees in both ϕ and ψ, for J-coupling calculations involving backbone atoms (including H atoms) and the C_β atom of the alanine side chain of the central residue. We have calculated 13 ^{3}J couplings involving including all 12 that involve rotation about the ϕ and ψ torsional angles, seven ^{2}J couplings and four ^{1}J couplings involving backbone atoms (24 in all). Figure 1 illustrates the nuclei which we used in for the coupling calculations (we specifically calculated the J's between the colored atoms).

As several of the J-couplings proved to be a complex function of the ϕ and ψ angles, neither Karplus-type nor truncated Fourier series expressions proved adequate to accurately fit the calculated values to a general analytical equation. Therefore, we chose to interpolate the values of the J-coupling for any arbitrary pair of ϕ, ψ values that differ from an actual point of the 2D grid using the equation of the plane defined from the three nearest points of the two-dimensional grid. This triangulation has the advantage of yielding a continuous 2D grid of J coupling values. The 2D-grid was extended to the range of −210 to 210 degrees in each coordinate to properly account for the periodicity of the angular variables and to avoid discontinuities in the interpolation of the ϕ and ψ variables,. The accuracy of such interpolation scheme will be addressed later on. A short FORTRAN function that performs the interpolation has been written and is included in the Supplementary Material along with the 2D grids of calculated J values.

Results

Effect of basis et variation on J's

The calculation of scalar J-couplings can depend upon the quantum mechanical methods used. In particular J's have been shown to depend upon the basis set used in these

calculations. Helgaker et al.[27] have studied the convergence of some one and two-bond J-couplings at the MCSCF level for simple molecules such as HF or H_2O. They found that the convergence of the J-couplings with the basis set extension was not smooth for typical energy-optimized basis sets such as the cc-pVXZ or aug-cc-pVXZ series. Decontraction of the basis and systematic extension by adding extra s-type functions was necessary in order to properly account for the Fermi contact contribution. Peralta et al.[28] described similar behavior at the B3LYP level. However, as noted by Pecul and Helgaker,[29] the basis set limit should be easier to achieve by DFT than wavefunction methods such as MCSCF or CCSD, were the correlation effects are gained via excitations to virtual orbitals.

While one and two-bond J's have been reported to be quite sensitive to basis sets with significant oscillations[27,28] as the basis et becomes larger, the dependence of calculated ^{2}J ^{15}N-^{13}C couplings with the ϕ and ψ dihedrals in peptides correlates well with experimental values.[30] Also trans H-bond ^{13}C-^{15}N scalar ^{3}J couplings have little basis set dependence. Reasonably good accuracy can be achieved using D95** with the B3LYP functional.[22]

We have performed full geometry optimizations at the B3LYP/D95** level for nine conformations about the central alanine residue of the acetyl-Ala_3-NH_2 model listed in table 1, including the four considered in table 2, to validate the procedure for obtaining the J-couplings we report. We, then, calculated the most representative ^{3}J, ^{2}J and ^{1}J couplings for each conformation using different basis sets. Table 2 presents these J couplings calculated using basis sets of increasing size including D95** and the cc-pVXZ-su0 family of basis sets for X=D,T,Q, described by Helgaker *et al.*[27] where the *s* functions of the original cc-pVXZ basis set are fully decontracted.. Due to computational limitations, we have used a combined basis set where the backbone and H atoms of the central residues use the quadruple-zeta and the remaining atoms the triple-zeta basis set in place of the largest cc-pVQZ-su0 basis set. For the small systems considered by Helgaker *et al.*, the ^{1}J and ^{2}J couplings obtained using the cc-pVXZ-su0 basis set family varied monotonically with increasing basis set size, making extrapolation to the complete basis set limit (CBS) possible.[27] The results of Table 2 indicate the extrapolation the to CBS worked only for some ^3J couplings in this study. We observed virtually no basis set dependence for $^2J(N_{11},C_{16})$. Importantly, the modest D95** basis set yields results similar to those of cc-pVTZ-su0 and close to our best estimate in most cases. The $^2J(C_{13}N_{21})$ and $^3J(H_{12}H_{14})$ couplings are exceptions. Nevertheless, the D95** calculations overestimate the ^{2}J coupling by roughly 0.6 Hz, or <10% of the absolute value. The more significant errors for the ^{3}J coupling (between 1.4 and 2.1 Hz or 20% too small) nevertheless remain roughly proportional to the correct value which varies between 3 and 10 Hz as a function of conformation. Where CBS extrapolations were possible, there were no significant differences between the extrapolated J couplings using a standard X^{-3} formula and those obtained with the cc-pVQZ-su0 basis set. Furthermore, since the J couplings didn't generally show monotonic behavior with increasing basis set size, we use the cc-pVQZ-su0 values as reference for a more comprehensive analysis of basis set effects.

Table 3 presents a comparison of 16 J couplings (two ^{1}J, four ^{2}J and ten ^{3}J couplings between backbone atoms, including the C_β nucleus and H atoms, involving at least one of the ϕ and ψ dihedral angles of the central residue) of the capped trialanine peptide calculated with the D95** and cc-pVQZ-su0 basis sets for the four conformations previously discussed.. The D95** basis set preforms surprisingly well. With the exceptions of $^1J(C_{13}C_{16})$, $^2J(C_{13},N_{21})$ $^3J(H_{12},H_{16})$ and $^3J(C_{13},H_{22})$, D95** gives the mean unsigned absolute errors (MUE) when compared to cc-pVQZ- su0 of <0.15 Hz. The small standard deviation values suggest the differences between the values obtained with the two basis sets to be systematic. The ^{3}J couplings involving the C_6 nucleus and $^1J(N_{11}C_{13})$ are particularly

insensitive to basis set effects. D95** systematically overestimates $^{1}J(C_{13}C_{16})$ by roughly 2 Hz, or 4% and $^{2}J(C_{13}N_{21})$ by 0.6 Hz, or 6%.

Two couplings, $^{3}J(H_{12},H_{14})$ and $^{3}J(C_{13},H_{22})$ present problems. The 1.5Hz MUE and 0.27 σ for the former, the only J coupling involving two H nuclei, are the largest of all couplings considered, suggesting that only large basis sets can correctly describe the electron density near the proton essential to the Fermi contact term. The MUE for $^{3}J(C_{13},H_{22})$ is small (0.16 Hz) in absolute value, but large compared to the small value (<1Hz) rendering the relative errors significant. We note that, while this coupling does not directly involve either of the two dihedral angles of the central residue, we have included it in this the study, as it is practically the only ^{3}J coupling used in the literature to probe dependence on ψ. This is probably because the other ^{3}J couplings that involve ψ, $^{3}J(N_{11},N_{21})$ $^{3}J(H_{14},N_{21})$ and $^{3}J(C_{15},N_{21})$, are small, typically <1 Hz in absolute value (see Table 3).

Quality of the interpolation

As noted above, we use an interpolation scheme to estimate J couplings from any pair of (ϕ,ψ) diedral angles. To check the accuracy of these interpolations we compare the J's calculated using the nine optimized conformations mentioned previously (none of which were used to build the 2D grid of J couplings), with the corresponding values obtained using the grid interpolation. Since we optimized all internal coordinates except for the ϕ and ψ dihedral angles, these coordinates could differ from those derived from the extrapolation. Thus, the optimized structure and that obtained from the interpolation could be qualitatively different (for example, by the formation of an internal H-bond), which could affect the couplings that are intrinsically dependent on geometrical parameters other than the ϕ and ψ dihedrals of the central residue.

Table 4 presents the maximum and average deviations over the nine conformations of the 17 J's directly involving the dihedral angles of the central residue. The overall accuracy of the interpolation is quite good, with mean unsigned errors (MUE's) of 0.1 Hz or less in all cases. The largest differences observed correspond to ^{3}J couplings involving the H_N nucleus of the central residue for a conformation in the vicinity of the left-handed alpha helical region of the Ramachandran plot, with dihedral angles (57,47). The calculated value of the $^{3}J(H_{12},H_{14})$ coupling is 4.53 Hz, compared to 4.24 obtained from interpolation. For the same conformation, calculated and interpolated values of $^{3}J(H_{12},C_{15})$ and $^{3}J(H_{12},C_{16})$ differed by 0.17 and 0.20 Hz, respectively. For the other conformations the differences between the interpolated and calculated J-couplings were <0.15Hz in all cases including the large ^{2}J couplings. These results confirm the accuracy of the linear interpolation. However, problems might occur if the J's depend upon other geometrical parameters as might occur if H-bonds form at certain combinations of ϕ and ψ. Our report of the energies vs. the dihedral angles noted several H-bonded structures whose energies represented discontinuities on the surfaces.[16] We chose two of the H-bonded structures, both of which had lower energies than the global minimum for the non-H-bonding structures on the potential energy surface which includes aqueous solvation. Using the notation of ref. 16, C10C10r contains two H-bonds, one between H_{22} and O_{30}, and another between O_{10} and the amino-terminal group. The central residue is in a helical region of the Ramachandran plot, with dihedrals (−67.3,−10.8). The other, C10rC7eq, has similar ϕ and ψ angles (−87.9, −5.1), but the second H-bond involves O_{22} instead of O_{30}. As seen from Table 5, the J couplings calculated for these (optimized) structures differ more substantially than those presented in Table 4 for those calculated using from the grid. The C10rC7eq structure has the larger error, probably as its H-bond directly affects the central residue. The effects of the H-bonds on the ^{1}J couplings, while significant in absolute value, produce errors of only ~5%.. However, the H-bond in C10rC7eq strongly affects the $^{2}J(N_{11},C_{16})$ and $^{2}J(C_{13},N_{21})$. Couplings calculated from the

optimized and interpolated values are −0.28 Hz and −0.90 Hz for the former, and −7.83 Hz and −8.84Hz for the latter. For the other ^{2}J couplings the relative errors remain below 5%.

The ^{3}J couplings involving H_{12} are particularly sensitive both to the presence of hydrogen bonds, and the orientations of the rest of the peptide. For both H-bonded structures, the neighboring ψ (about the C_3-C_6 bond) and ϕ (about the N_{21}-C_{23} bond) of about −15 and −85 degrees, respectively, differ significantly from those (about 170 and −155) of the conformations used to make the grid, respectively. Conversely, the ^{3}J couplings involving the C_6 atom are relatively insensitive to variation of the ψ dihedral angle (about the C_3-C_6 bond). Table 5 also includes the J's calculated with the extended basis set for comparison with d95**. We found the differences between these values to be similar to the average errors of Table 3 confirming that the presence of H-bonds does not adversely affect the performance of the D95** basis set.

Coupling constants

^{3}J coupling constants—Figures 2–22 display the results of the calculations as functions of the dihedral angles ϕ and ψ in the format of Ramachandran plots. In each of these figures, the angle ψ is plotted vertically and ϕ, horizontally, conforming to normal usage. The contours for the J's in Hz are labeled in the legends. If the J's be functions of only one dihedral angle (either ϕ or ψ, but not both) as predicted by a Karplus-like relationship, these two dimensional plots should appear as stripes. However, if the J's be significantly influenced by both dihedrals, the figures should be more complex. Only three of the figures show the striped behavior expected for a pure (Karplus) dependance. These describe the ^{3}J(C_6-H_{14})(figure 2), the ^{3}J(C_6-C_{16}) (figure 3), the ^{3}J(C_6-C_{15}) (figure 4) all as a function ϕ. These plots are very similar to those obtained by Bax [2] using Karplus equations derived from NMR data of proteins. All of the others exhibit complex dependence on ϕ and ψ even in the most populated regions of the Ramachandran plot, such as the upper left quadrant. Bax has pointed out that the dihedrals involving H's can differ from those expected if the ω dihedral were exactly 0 or 180 degrees. Karplus, himself, noted that the relationship between J's and the dihedral angles can be affected by changes in bond angles and bond lengths,[31] both of which will change slightly with each optimized structure. As a result, the relationships between the J's and ϕ and ψ should be more complex than for the dihedrals involving only the C or N atoms (which are precisely ϕ and ψ),[2] as is the case for ^3J(H_{12}-H_{14}, figure 5) ^3J(H_{12}-C_{15}, figure 6)and ^3J(H_{12}-C_{16}, figure 7) which see wide use (especially the first) for protein structure determination based upon Karplus-type relationships about ϕ. [2] For example, the results of figure 5 predict the ^3J(H_{12},H_{14}) at ϕ =−60 degrees to be much smaller in the helical ψ = (0,−50) than in the polyproline region, around ψ = 150 degrees.

Of the few ^{3}J couplings that could be useful experimental probes for the ψ dihedral, we find those involving N_{11}, H_{14}, or C_{15}, with either N_{21} or O_{20} backbone atom atoms (Figures 8–14). The insensitivity of the ^{3}J(^{15}N-^{17}O) coupling to both dihedrals (figure 9) except for the small region at (180,180) together with its small value and the difficulty of measurement render this J rather useless for structure determination. Other couplings involving the O_{20} atom (Figures 8 and 10) span a larger range of values and strongly depend both on ψ, as expected, and ϕ. However, these are not experimentally useful since the ^{17}O quadrupole moment and fast relaxation make accurate measurements of these small J's quite difficult. The small range of values for ^{3}J(^{15}N-^{15}N) and ^{3}J(^{13}C-^{17}O) (figures 8 and 11) reduces the utility of these J's, as well leaving only ^{3}J(H_{14},N_{21}) (Figure 12) as a useful experimental measure. The ^{3}J($C_{13}H_{22}$) 's, which correlate with ψ according to an experimental report,[3] are useful for structure determination,[8] in good agreement with our calculations (note the strong dependence on ψ, and weak dependence on ϕ in figure 13). Millhauser[32] has

reported $^3J(H_{12}H_{14})$'s for helical polyalanines that are consistent with the H-bonding minima that we reported for alanines[16] and the J's of figure 5.

^{2}J coupling

Figures 15 and 16 depict the dependence on ϕ and ψ for two geminal ^{2}J's involving backbone atoms. Each depends on both backbone dihedral angles in a complex manner. Hennig has proposed $^2J(C_{13},N_{21})$ for use in protein structure determination.[3] In fact, *ab initio* calculated ^{2}J ^{13}C-^{15}N (C_{13}-N_{21}) couplings (figure 15) have been shown to give a better fit to ubiquitin structure than a simple Karplus-like equation.[4,30] The results of figure 15 strikingly resemble those reported by Kozminski *et al.*[30] both qualitatively and quantitatively.

Juranic et al. have investigated the use of $^2J(N_{11},C_{16})$.[6] The other ^{2}J couplings have rarely been considered. However, Schmidt *et al.* recently reported an attempt to correlate all ^{2}J couplings we have considered in this paper with protein secondary structure after extensive experimental measurements.[33] In general, the range of experimental values they obtained agrees well with our *ab initio* calculations. An exception is the $^2J(H_{12},C_{13})$ coupling, which ranges from 0 to 4.5 Hz (see Figure 20) in contrast to the −4 Hz to +8 Hz range measured by Schmidt. The $^2J(C_{13},N_{21})$ coupling behaves similarly, however the range of values we obtained for this coupling agrees with the measurements of Ding et al.[4] As the C_6-H_{12} and H_{14}-C_{16} ^{2}J's both exhibit substantial variation with both dihedrals, they could potentially be used for structure determination.

^{1}J coupling

While we have less confidence in the calculated values of the ^{1}J couplings as their dependences upon the dihedrals may be secondary effect, both C_{13}-C_{16} (figure 22) and N_{11}-C_{13} (figure 23) J's show substantial variation with both dihedral angles.

DISCUSSION

As noted, the calculated J's discussed in this paper are based on interpolations of the Ramachandran map of optimized structures of acetyl$(Ala)_3NH_2$ previously published.[16] These structures were individually optimized for fixed values of ϕ and ψ. This energy map seems to be an improvement over those that only consider one capped amino acid as it explains why few structures are found experimentally in the Ramachandran allowed region near ψ = −30 to −80 and ϕ = −150 to -180 degrees.[34]

As can be seen from the various figures, the coupling constants often depend upon more than one of the two dihedral angles that we have considered. The three exceptions, the ^3J (C_6-H_{14}), ^3J (C_6-C_{15}) and ^3J (C_6-C_{16}) appear to depend chiefly on ϕ, with little contribution from ψ. All of the other J's depend somewhat on both dihedrals. The ^{3}J (C_{13}-H_{22}) coupling appears to depend upon the ϕ and ψ angles despite the fact that the rotation about either of these angles does not directly affect the spatial relationship between atoms 13 and 22. We believe that these dependencies might be due to a secondary effect resulting from the optimization of all the other geometrical parameters for each fixed vale of ϕ and ψ. The dihedral angles other than ϕ and ψ that are fixed at each grid point could vary considerably with small changes in the fixed dihedrals that define the grid and small differences in bond lengths and bond angles might result from optimizations at different values of the dihedrals. For example, the formation and breaking of intramolecular H-bonds could cause almost discontinuous changes in the optimized parameters as the angles are incrementally changed. As noted above, the J's of the two H-bonded structures have larger than normal deviations from the values for the corresponding dihedrals using the extrapolation. We cannot

determine if this observation be due to the H-bonds themselves, or to the secondary dihedrals and bond length and angle changes. Nevertheless, this ^{3}J coupling has been used in some experimental correlations of J's with protein structure,[3,8] so we include this data for completeness. Perhaps structural fits to J's should take the possibility of such H-bonding structures specifically into account.

While the calculated ^{2}J and ^{1}J couplings might be intrinsically less reliable than those for the ^{3}J coupling, Kozminski, et al., have convincingly shown the advantage of using ^{2}J (C_{13}-N_{21}) as a function of both ϕ and ψ instead of ψ alone.[30] Furthermore, Kozminski, et al.'. calculated dependence upon ϕ and ψ (figure 5 of the reference) strikingly resembles that presented here (figure 15) both qualitatively and quantitatively. The other ^{2}J couplings all exhibit clear dependencies on both ϕ and ψ, so they may be useful for structure determination. However, we note that the ^{2}J coupling C_6-H_{12} should only have secondary dependence on ϕ and ψ in the manner noted above for the ^{3}J coupling between C_{13} and H_{22}.

Rather than attempt to fit analytical functions in ϕ and ψ to the data corresponding to each Ramachandran-like map, we have chosen to write a small program (included in the SI) that will interpolate the surfaces for any combination of ϕ and ψ for any of the couplings studied. The interpolation works quite well as seen from tables 4 and 5. We provide this data so that we and others can use these calculated data together with experimental J's used alone or in conjunction with other experimental data to help determine the conformations of proteins and peptides in solution using nmr.

CONCLUSION

We find many J's associated with the backbones of peptides and proteins to be functions of both the ϕ *and* ψ dihedrals, rather than simply ϕ *or* ψ. The data resulting from the calculations reported here can be used to more accurately determine peptide and protein structures from nmr measurements in solution. A small program that will interpolate the values of each J considered together with the associated data is available from the authors.

Acknowledgments

This work was supported by a National Institute on Aging grant (SC1AG034197). P.S. acknowledges partial support from grant MAT2008-04834. Some calculations used the CUNY Graduate School Research Computing Cluster.

REFERENCES

1. Karplus M. J. Chem. Phys. 1959; 30:11.
2. Hu J-S, Bax A. Journal of the American Chemical Society. 1997; 119:6360.
3. Hennig M, Bermel W, Schwalbe H, Griesinger C. Journal of the American Chemical Society. 2000; 122:6268.
4. Ding K, Gronenborn AM. Journal of the American Chemical Society. 2004; 126:6232. [PubMed: 15149211]
5. Shi Z, Olson CA, Rose GD, Baldwin RL, Kallenbach NR. Proc. Nat. Acad. Sci U.S.A. 2002; 99:9190.
6. Juranic N, Dannenberg JJ, Cornilescu G, Salvador P, Atanasova E, Ahn H-C, Macura S, Markley JL, Prendergast FG. Protein Sci. 2008; 17:768. [PubMed: 18305196]
7. Juranic N, Macura S. J. Am Chem. Soc. 2001; 123:4099. [PubMed: 11457169]
8. Graf, Jr; Nguyen, PH.; Stock, G.; Schwalbe, H. Journal of the American Chemical Society. 2007; 129:1179. [PubMed: 17263399]
9. Markwick PRL, Showalter SA, Bouvignies G, Bruschweiler R, Blackledge M. Journal of Biomolecular NMR. 2009; 45:17. [PubMed: 19629714]

10. Atreya HS, Garcia E, Shen Y, Szyperski T. Journal of the American Chemical Society. 2007; 129:680. [PubMed: 17227032]
11. Neal S, Berjanskii M, Zhang H, Wishart DS. Magnetic Resonance in Chemistry. 2006; 44:S158. [PubMed: 16823900]
12. Makowska J, Rodziewicz-Motowidlo S, Baginska K, Vila JA, Liwo A, Chmurzynski L, Scheraga HA. PNAS. 2006; 103:1744. [PubMed: 16446433]
13. Gattin Z, Zaugg J, van Gunsteren WF. Chem Phys Chem. 2010; 11:830. [PubMed: 20162655]
14. Schweitzer-Stenner R. Journal of Physical Chemistry B. 2009; 113:2922.
15. Theis K, Dingley AJ, Hoffmann A, Omichinski JG, Grzesiek S. J. Biomol. NMR. 1997; 10:403. [PubMed: 20859784]
16. Tsai MI-H, Xu Y, Dannenberg JJ. J. Phys. Chem. B. 2009; 113:309. [PubMed: 19072621]
17. Salvador P, Kobko N, Wieczorek R, Dannenberg JJ. J. Am Chem. Soc. 2004; 126:14190. [PubMed: 15506785]
18. Frisch, MJ., et al. GAUSSIAN 03. Pittsburgh PA: Gaussian, Inc.; 2003.
19. Frisch, MJ., et al. Gaussian 09, Revision A.2. Wallingford CT: Gaussian, Inc.; 2009.
20. Becke AD. J. Chem Phys. 1993; 98:5648.
21. Lee C, Yang W, Parr RG. Phys. Rev. B. 1988; 37:785.
22. Salvador P, Dannenberg JJ. J. Phys. Chem. B. 2004; 108:15370.
23. Helgaker T, Watson M, Handy NC. J. Chem Phys. 2000; 113:9402.
24. Sychrovsky V, Grafenstein J, Cremer D. J. Chem Phys. 2000; 113:3530.
25. Barone V, Peralta JE, Contreras RH, Snyder JP. Journal of Physical Chemistry A. 2002; 106:5607.
26. Ramsey NF. Phys. Rev. 1953; 91:303.
27. Helgaker T, Michal Jaszunaski, Ruud K, Gorska A. Theoretical Chemistry Accounts. 1998; 99:175.
28. Peralta JE, Scuseria GE, Cheeseman JR, Frisch MJ. Chem. Phys. Lett. 2003; 375:452.
29. Pecul M, Helgaker T. International Journal of Molecular Sciences. 2003; 4:143.
30. Kozminski W, Zhukov I, Pecul M, Sadlej J. J. Biomol. NMR. 2005; 31:87. [PubMed: 15772749]
31. Karplus M. Journal of the American Chemical Society. 1963; 85:2870.
32. Millhauser GL, Stenland CJ, Bolin KA, Ven FJMvd. J. Biomol. NMR. 1996; 7:331. [PubMed: 8765739]
33. Schmidt JM, Hua Y, Löhr F. Proteins: Structure, Function, and Bioinformatics. 2010; 78:1544.
34. Perskie LL, Street TO, Rose GD. Protein Science. 2008; 17:1151. [PubMed: 18434497]

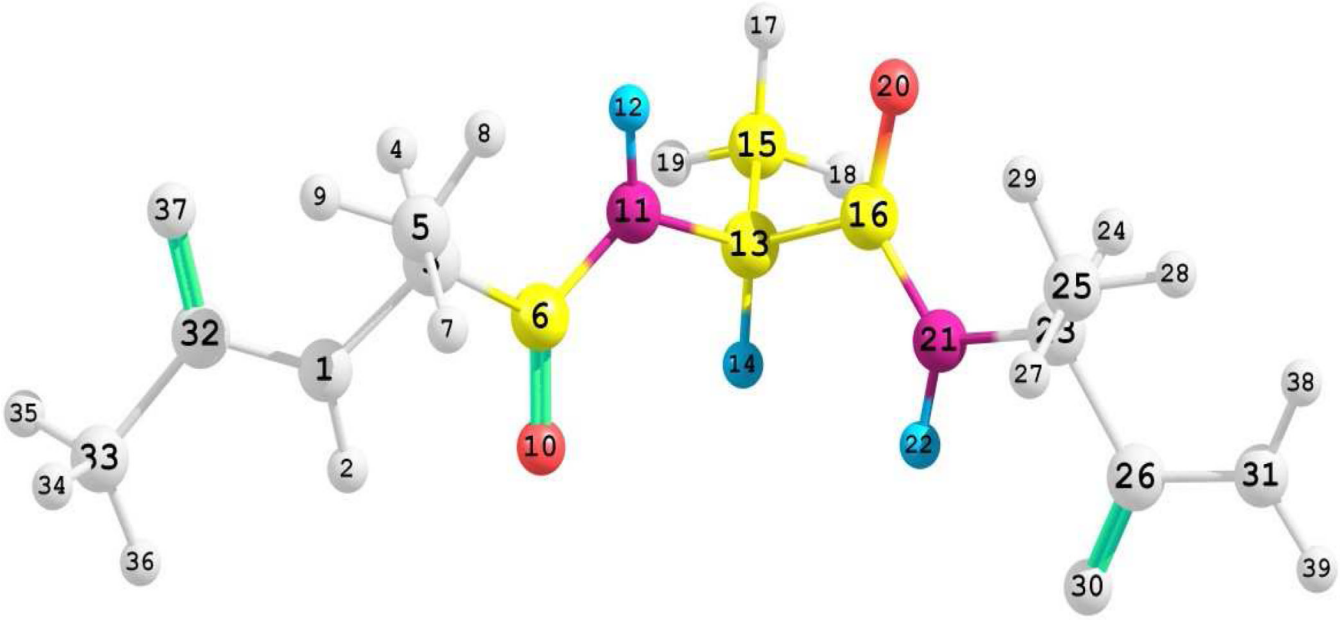

Figure 1.
Numbering scheme used for acetyl$(ALA)_3NH_2$. Colored atoms are those activated for the calculation of J's.

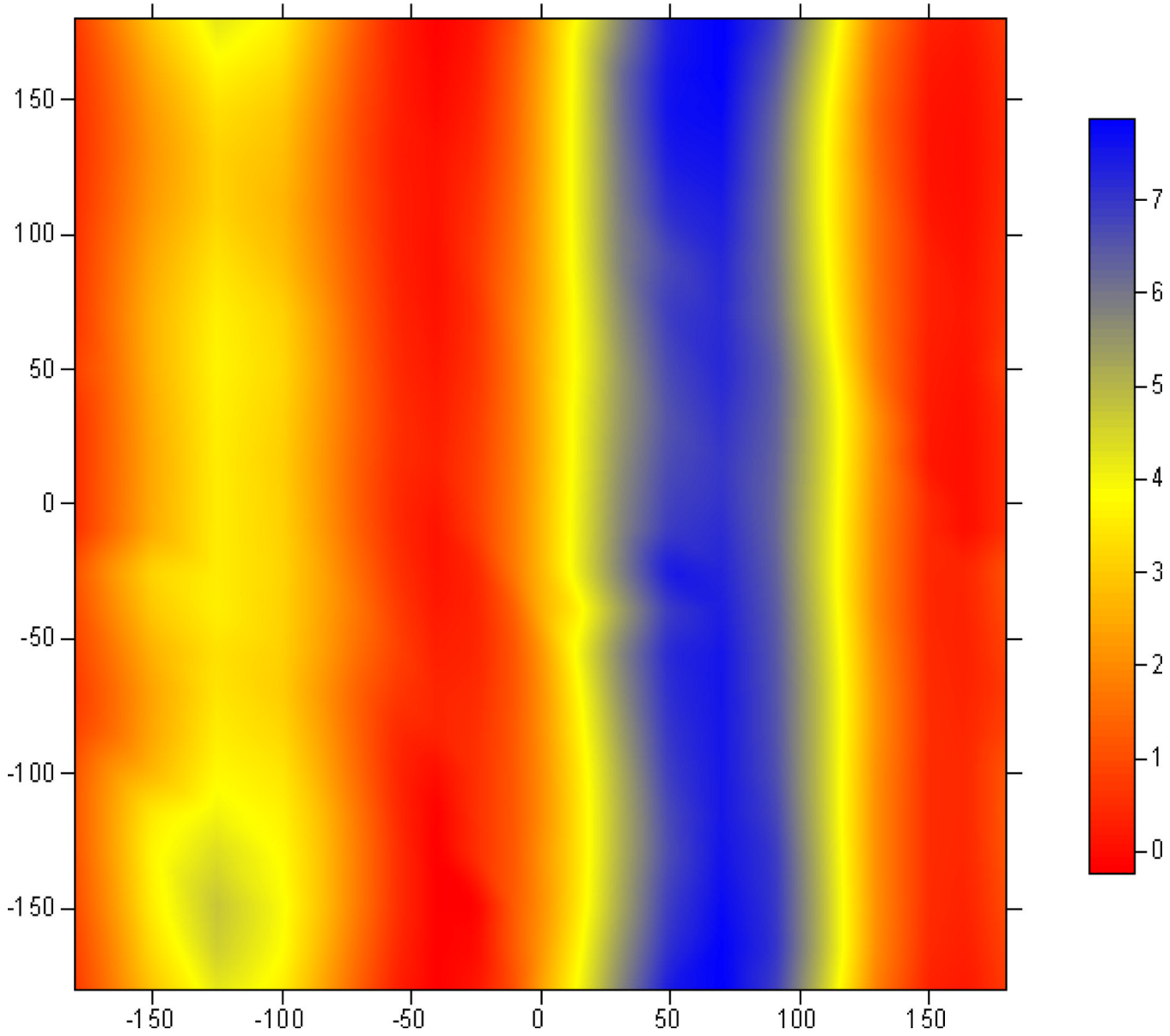

Figure 2.
$^{3}J(C_6\text{-}H_{14})$ as function of ϕ and ψ.

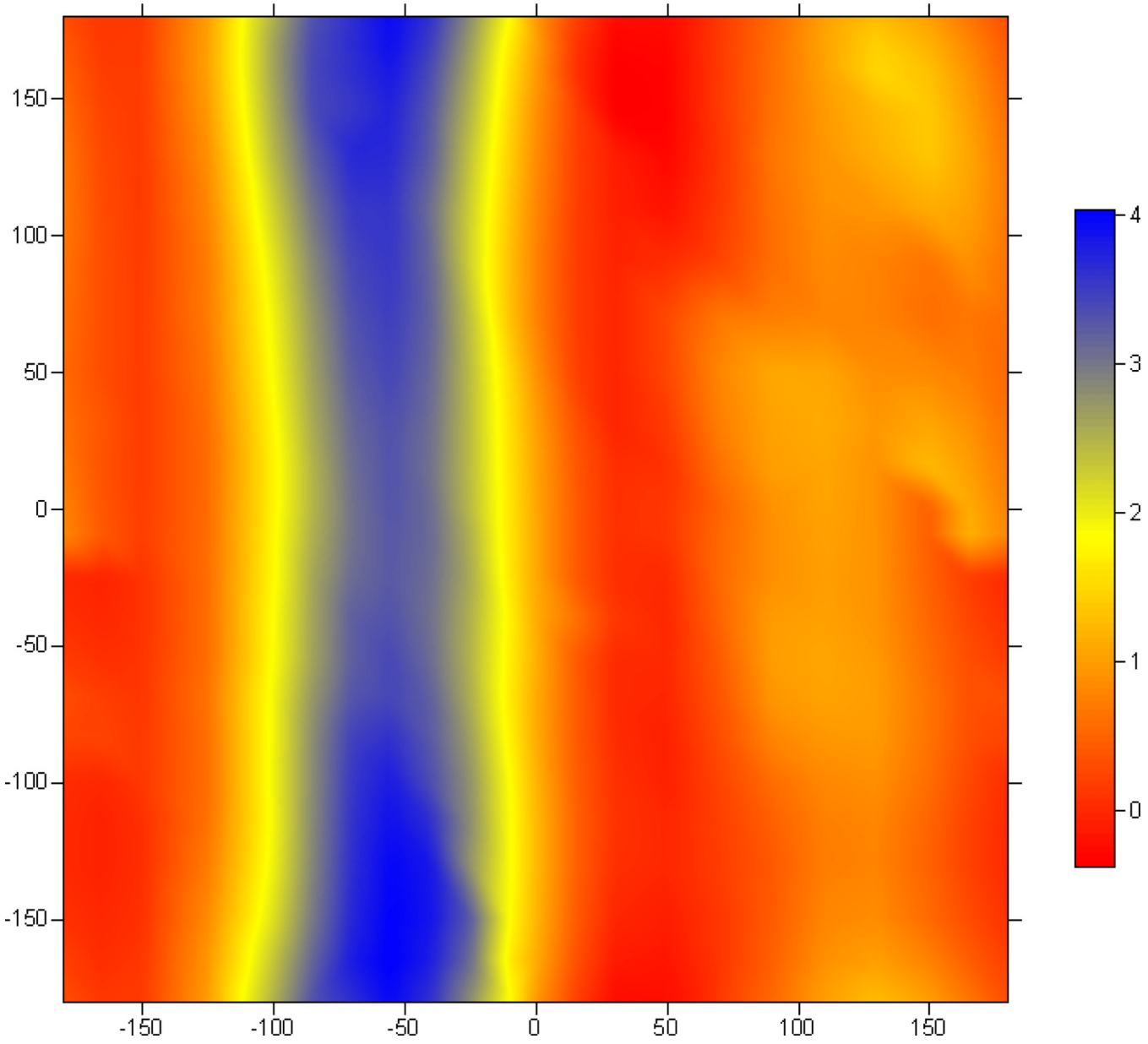

Figure 3.
$^{3}J(C_6\text{-}C_{15})$ as function of ϕ and ψ.

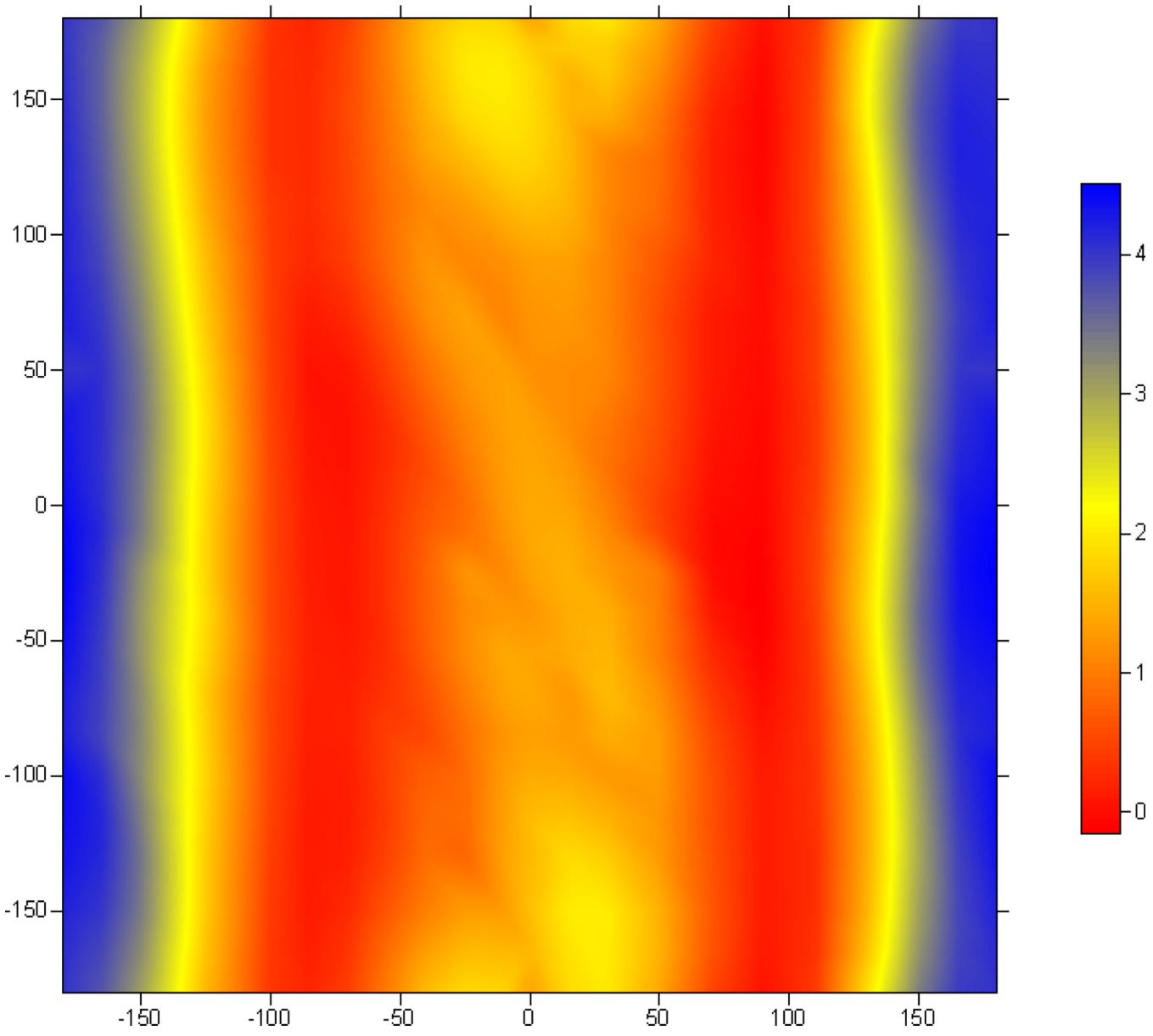

Figure 4.
$^{3}J(C_6,C_{16})$

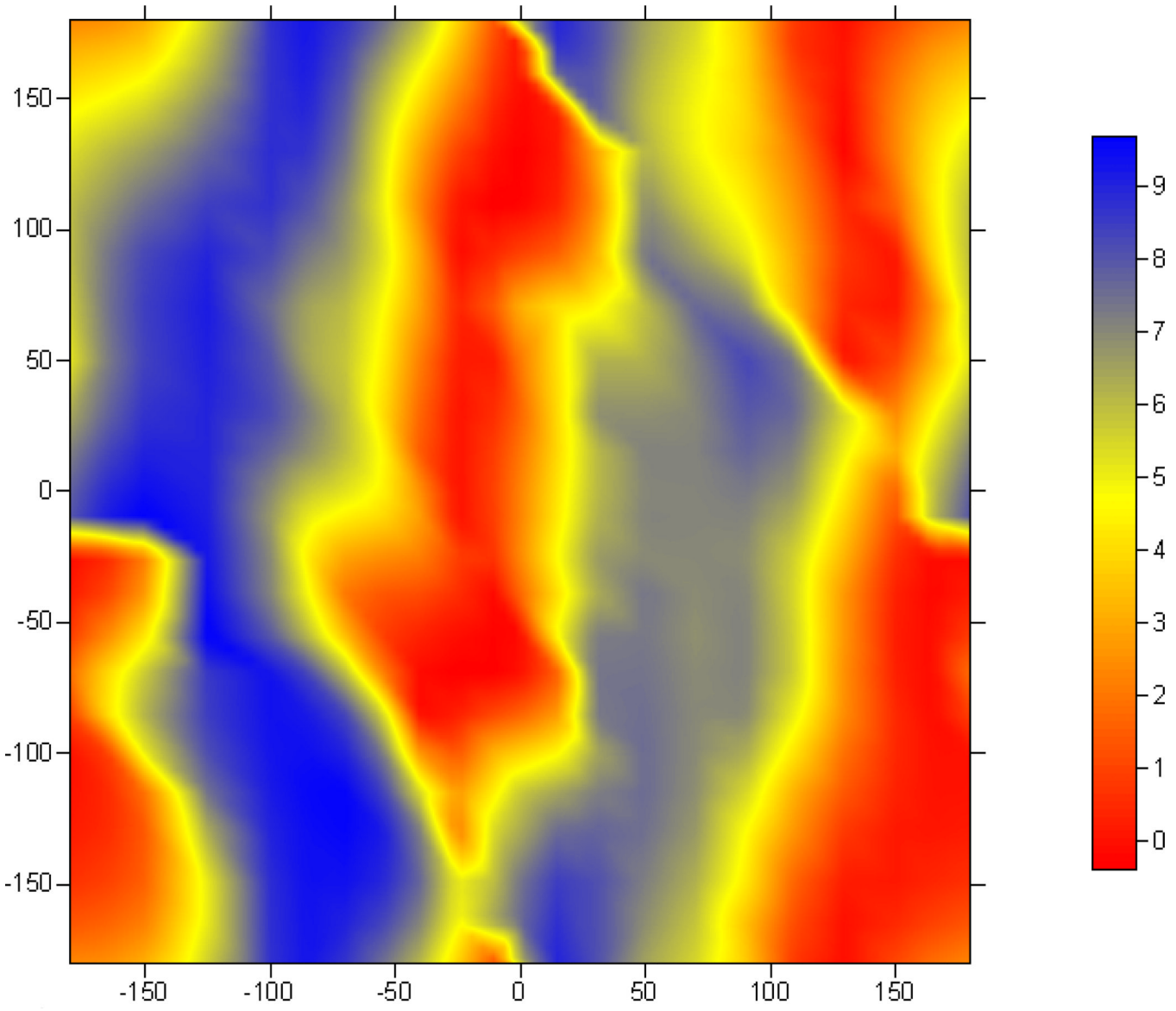

Figure 5.
$^{3}J(H_{12},H_{14})$

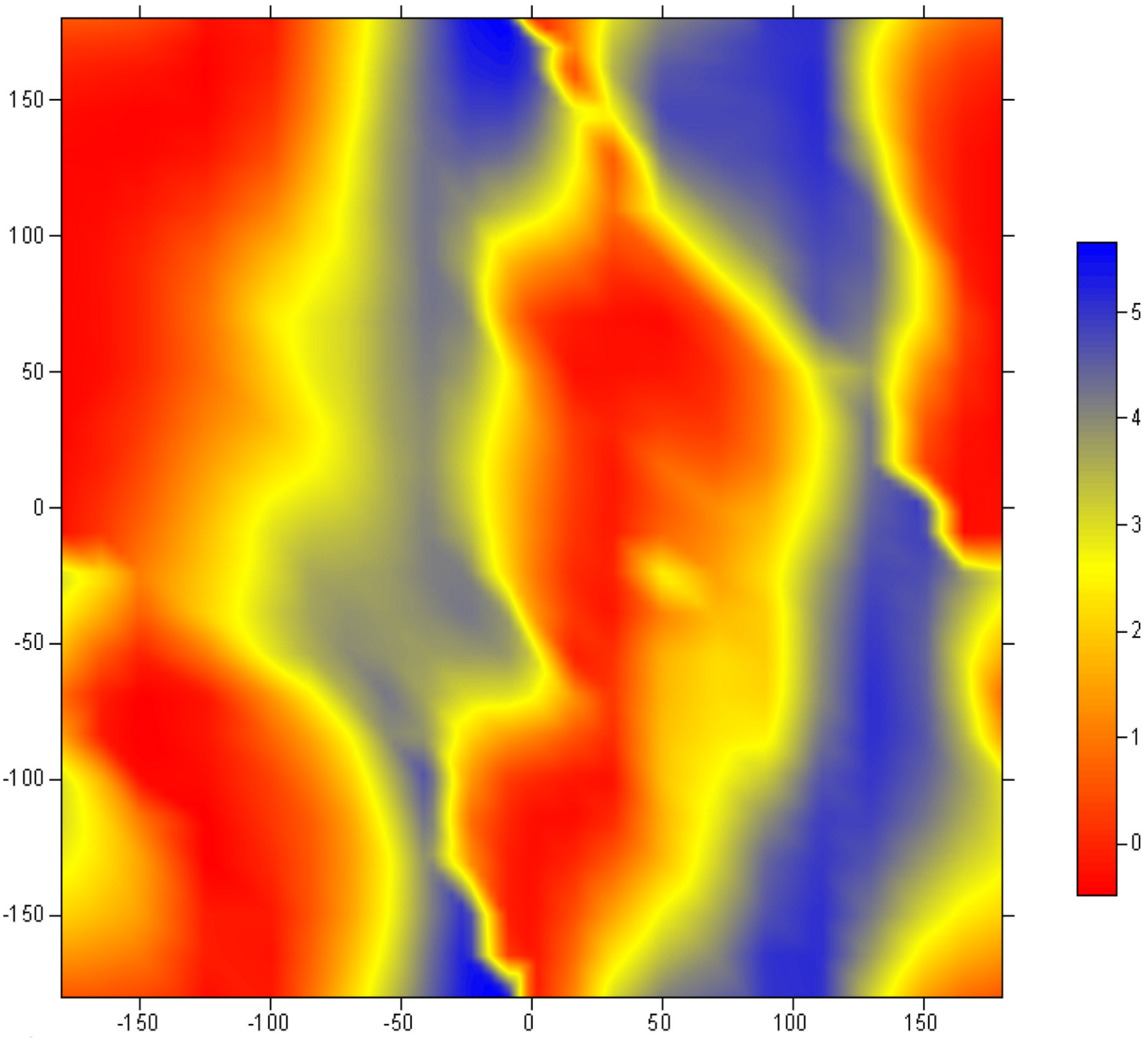

Figure 6.
$^{3}J(H_{12}\text{-}C_{15})$

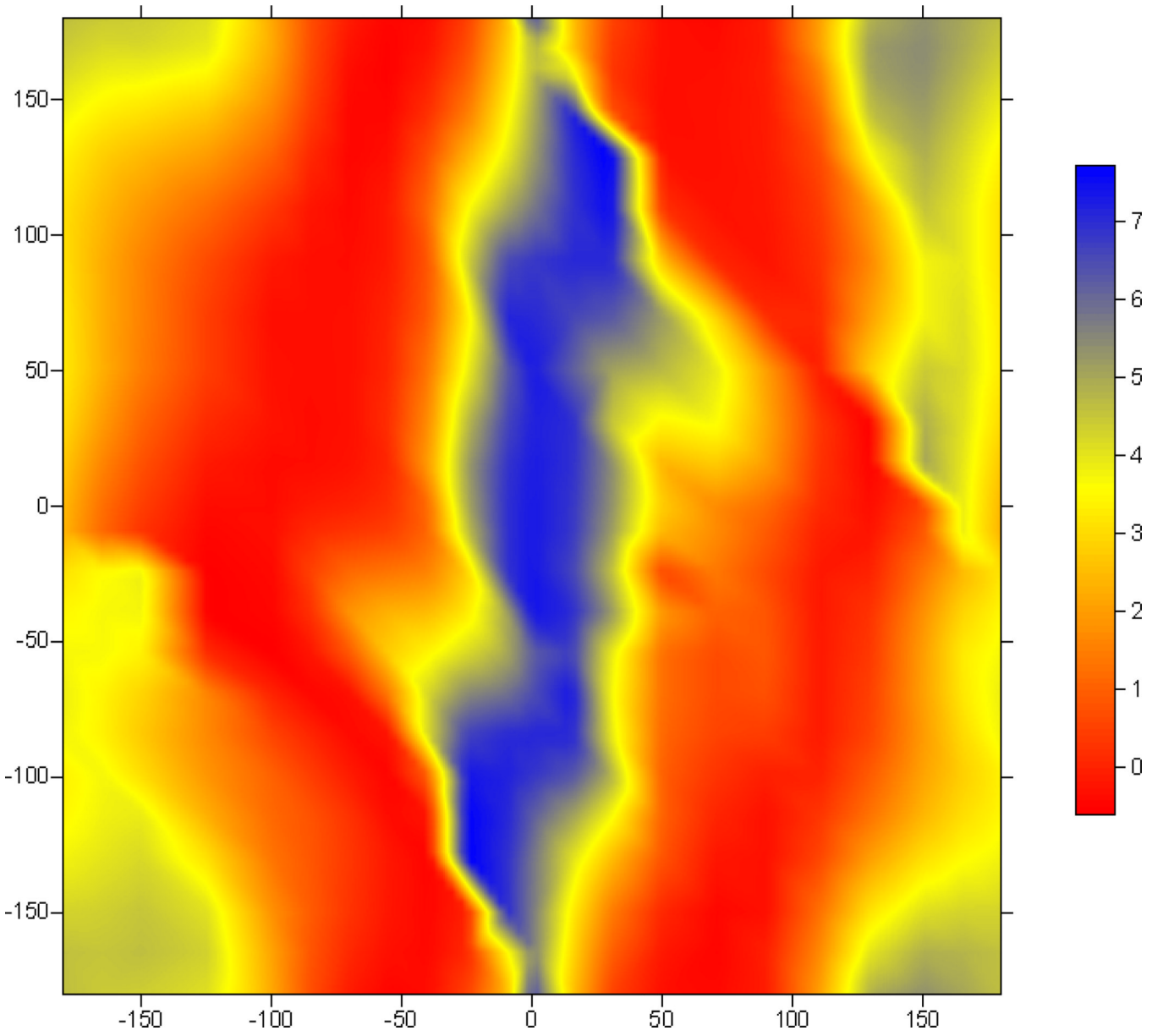

Figure 7.
$^{3}J(H_{12}\text{-}C_{16})$

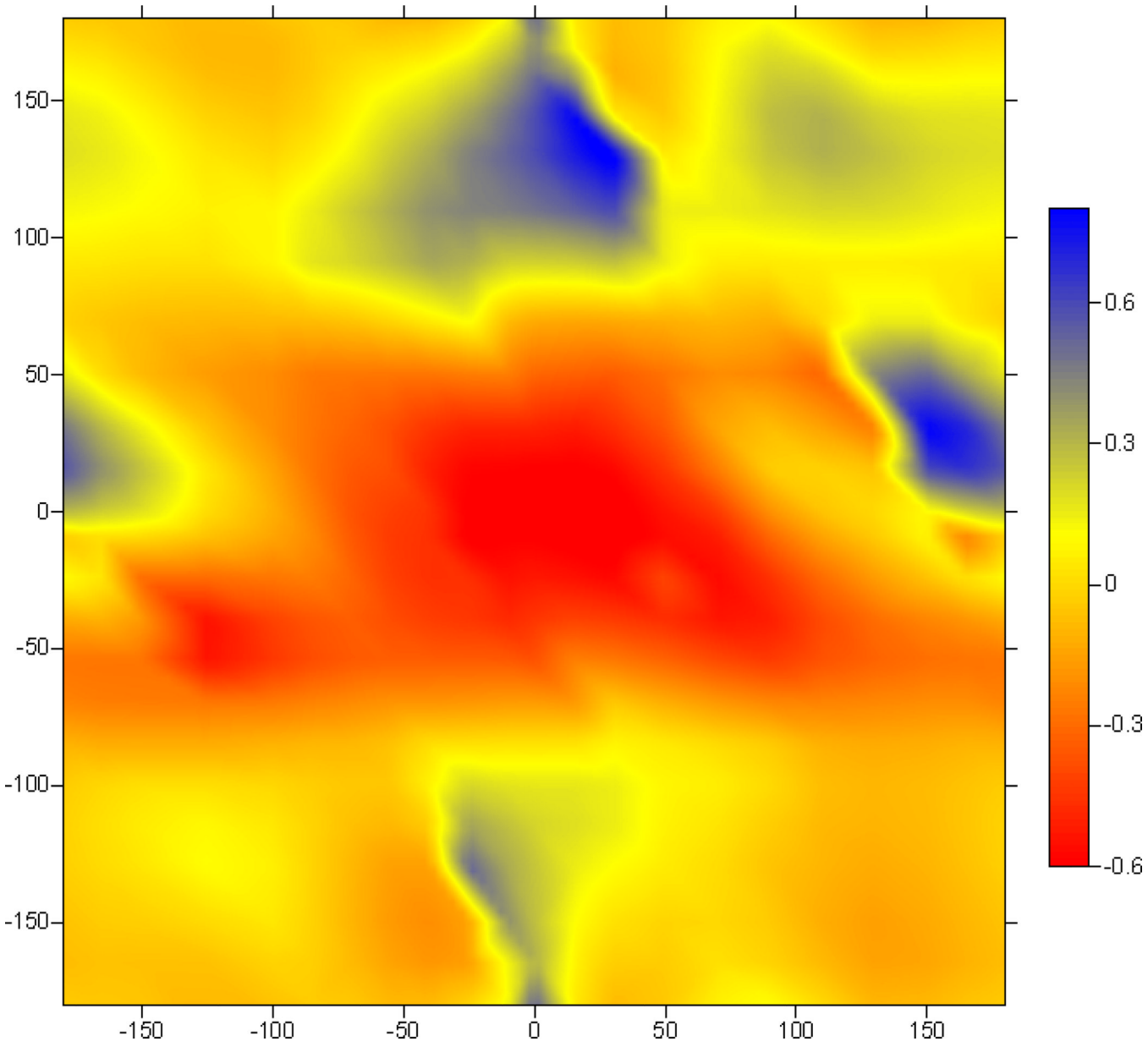

Figure 8.
$^{3}J(N_{11}\text{-}N_{21})$

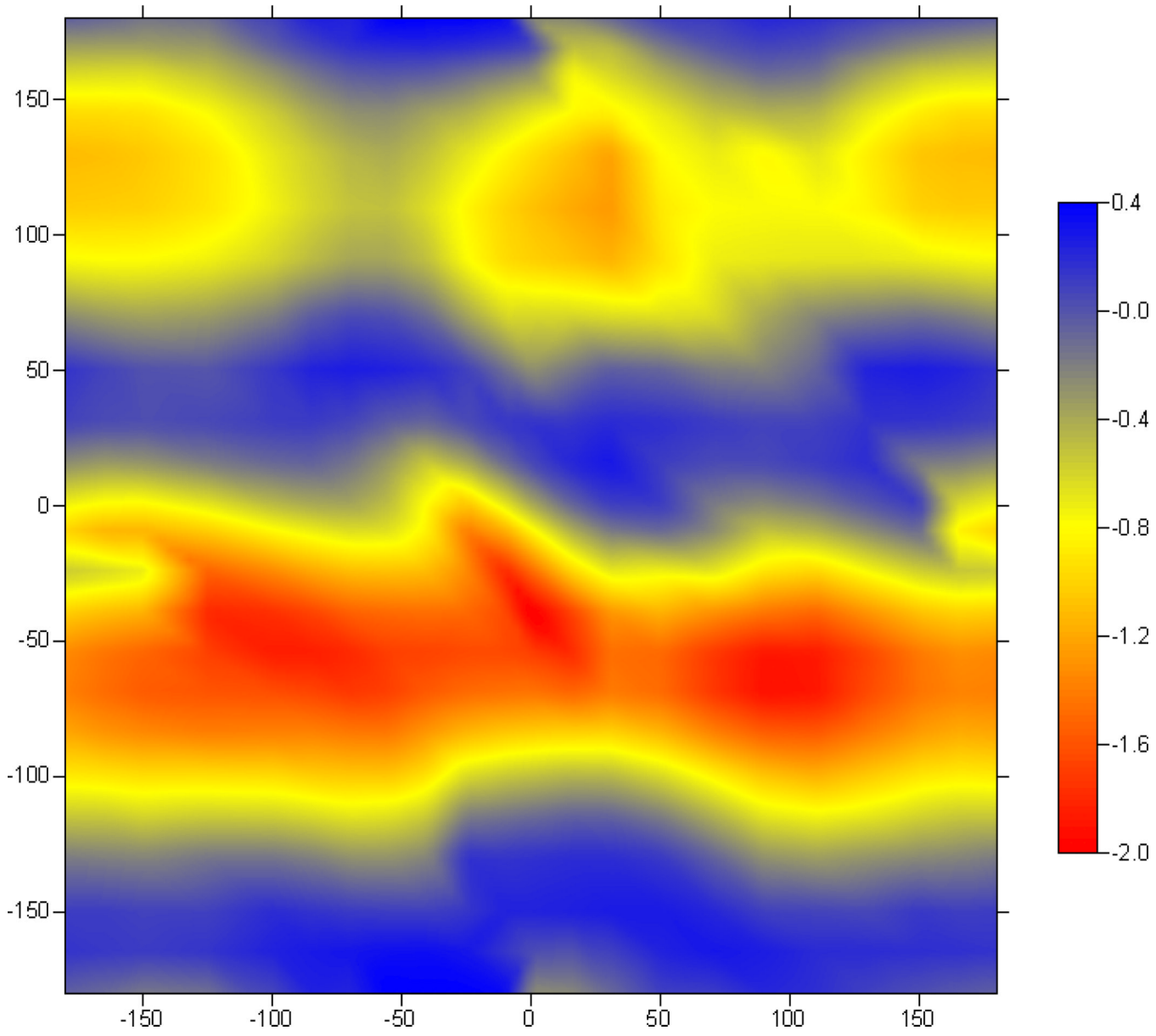

Figure 9.
$^{3}J(H_{14}\text{-}N_{21})$

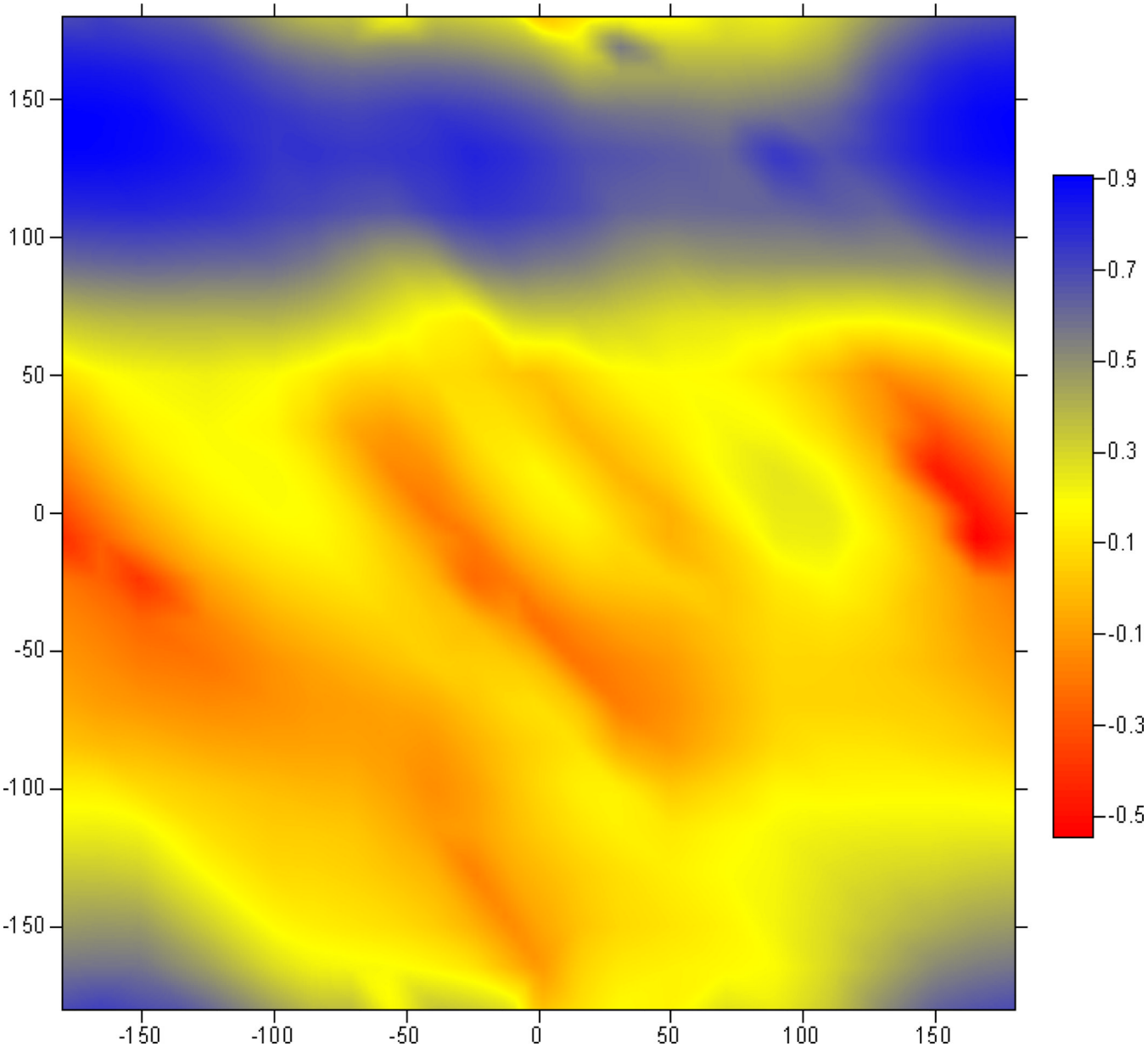

Figure 10.
$^{3}J(C_{13}\text{-}H_{22})$

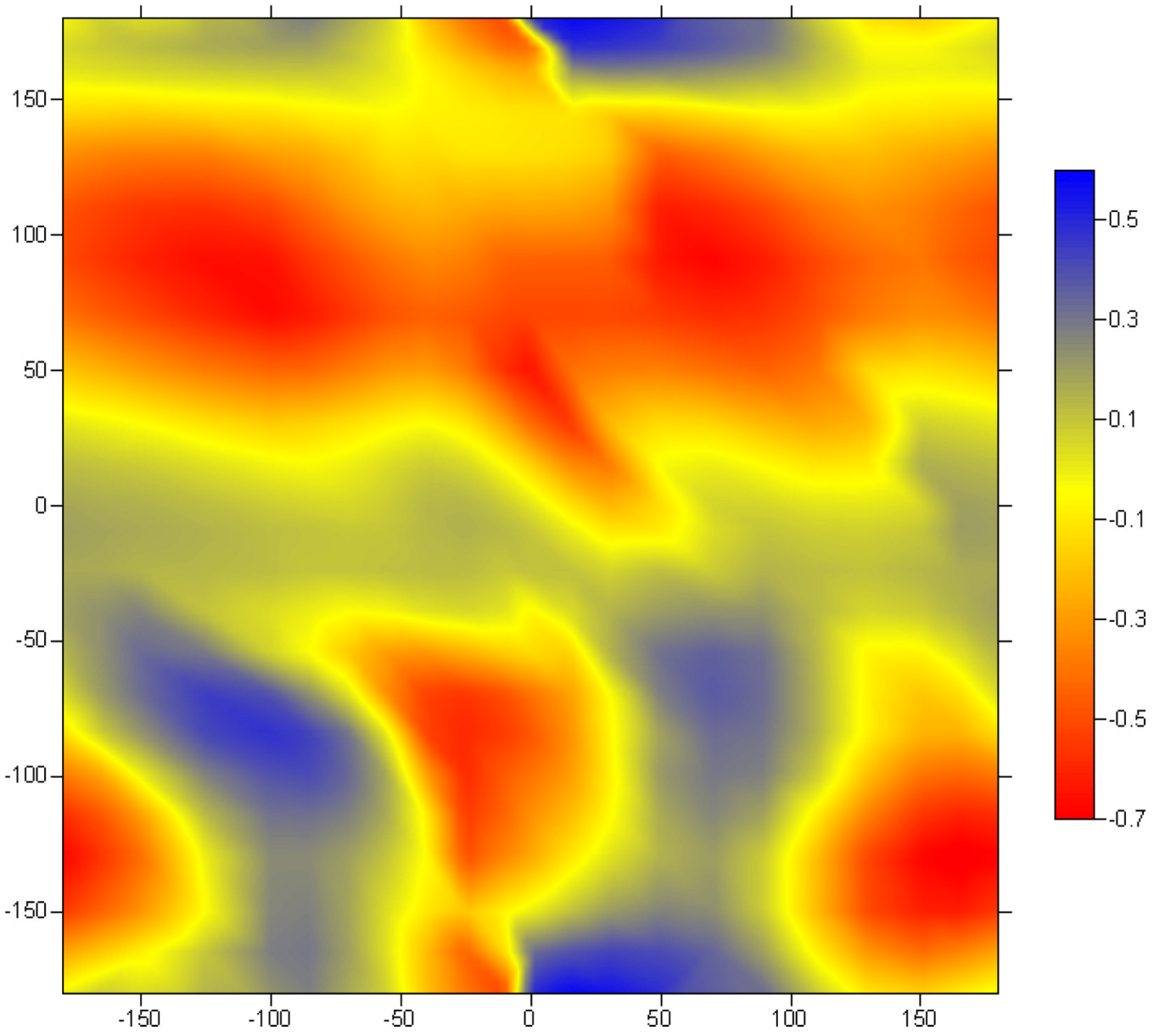

Figure 11.
$^{3}J(C_{15}\text{-}N_{21})$

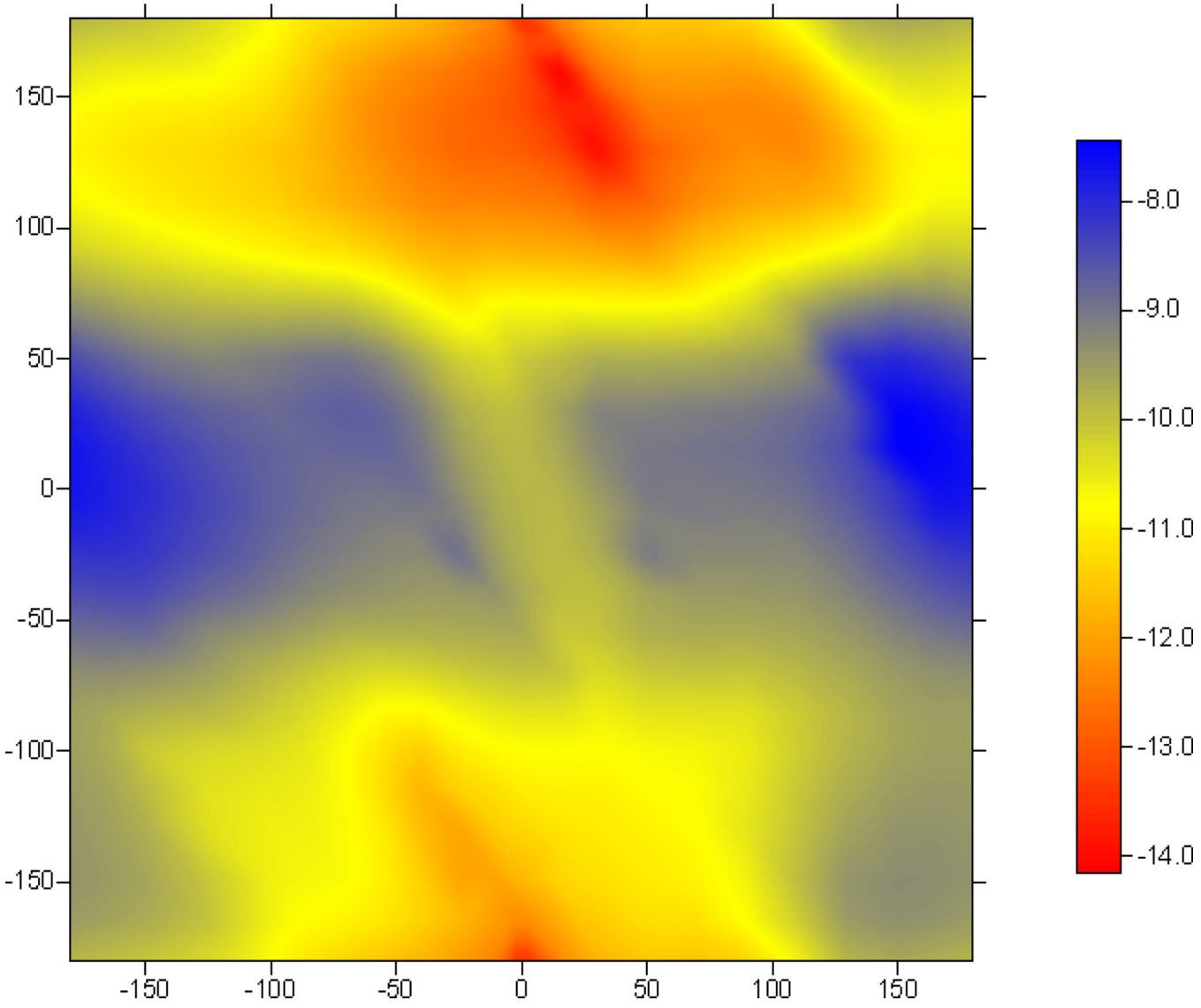

Figure 12.
$^{2}J(C_{13}\text{-}N_{21})$

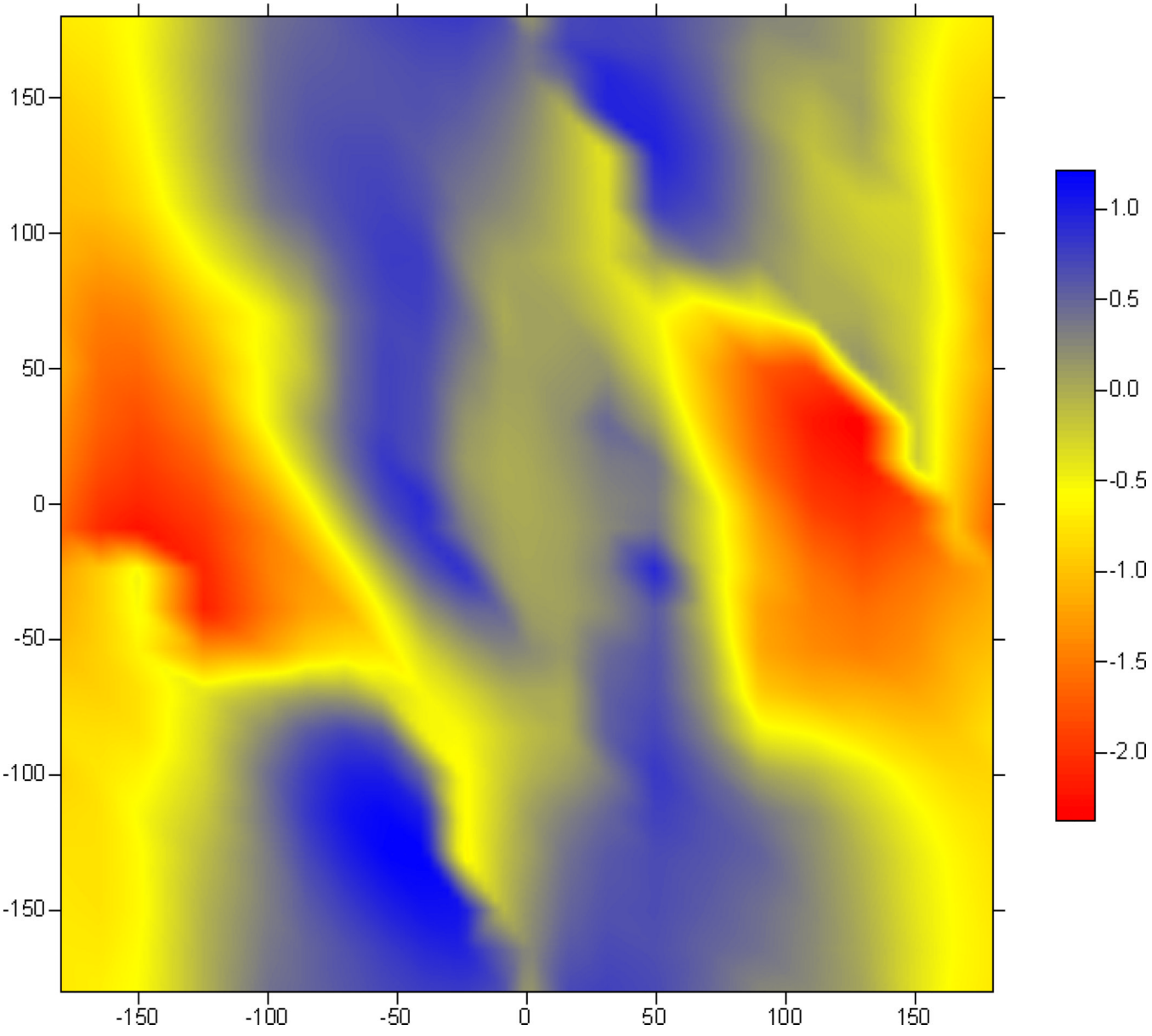

Figure 13.
$^{2}J(N_{11}\text{-}C_{16})$

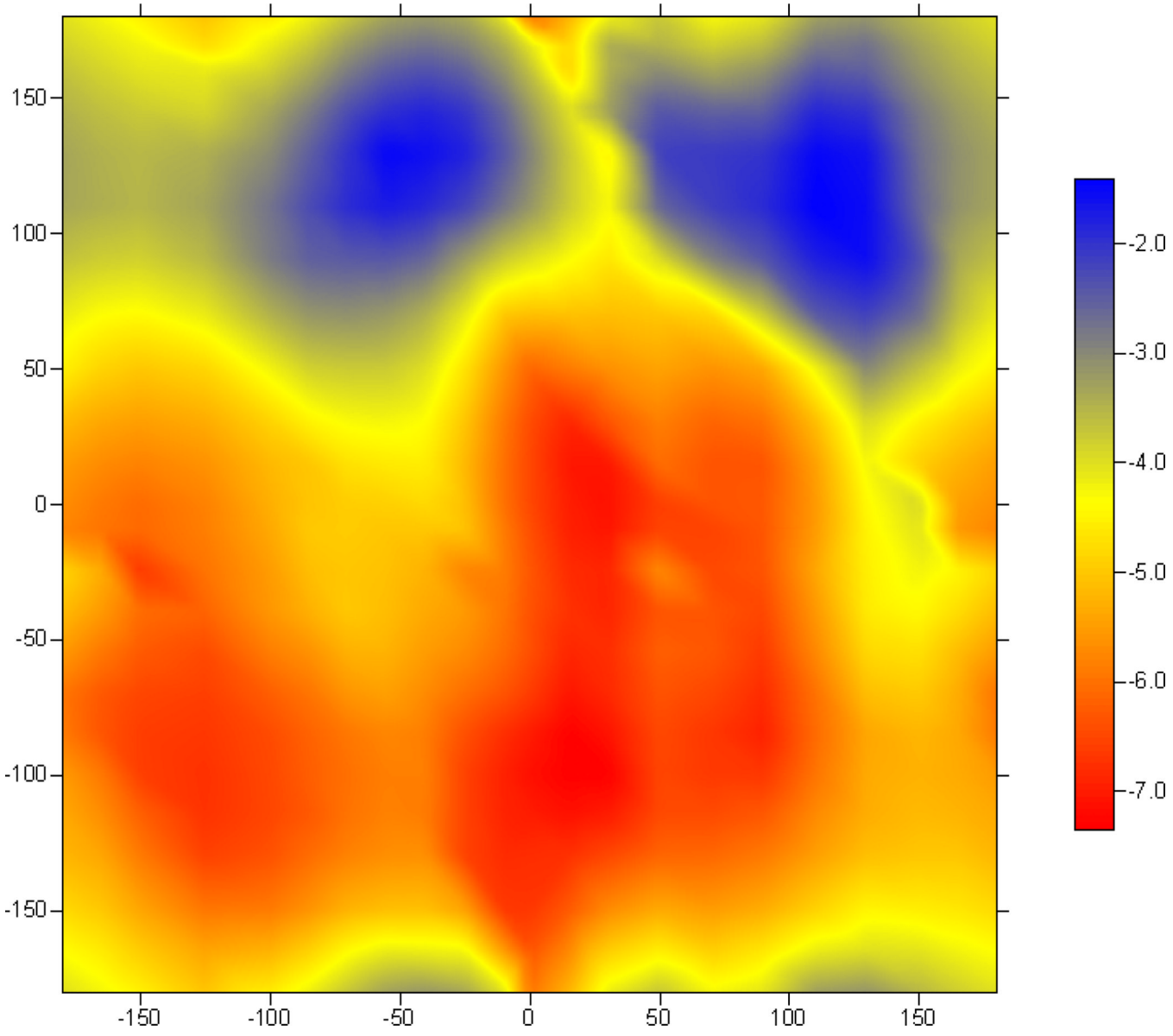

Figure 14.
$^{2}J(H_{14}\text{-}C_{16})$

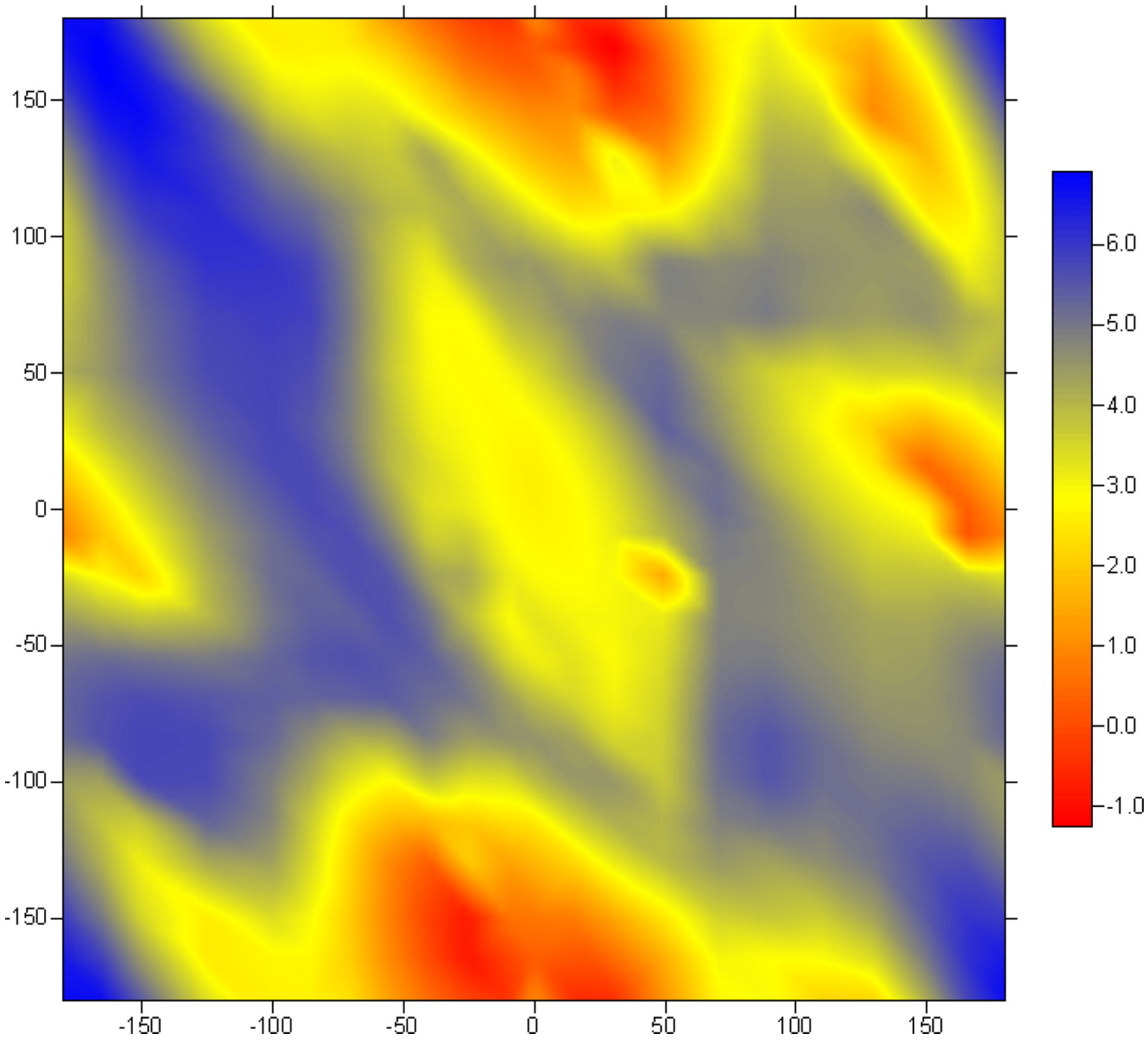

Figure 15.
$^{2}J(C_6\text{-}H_{12})$

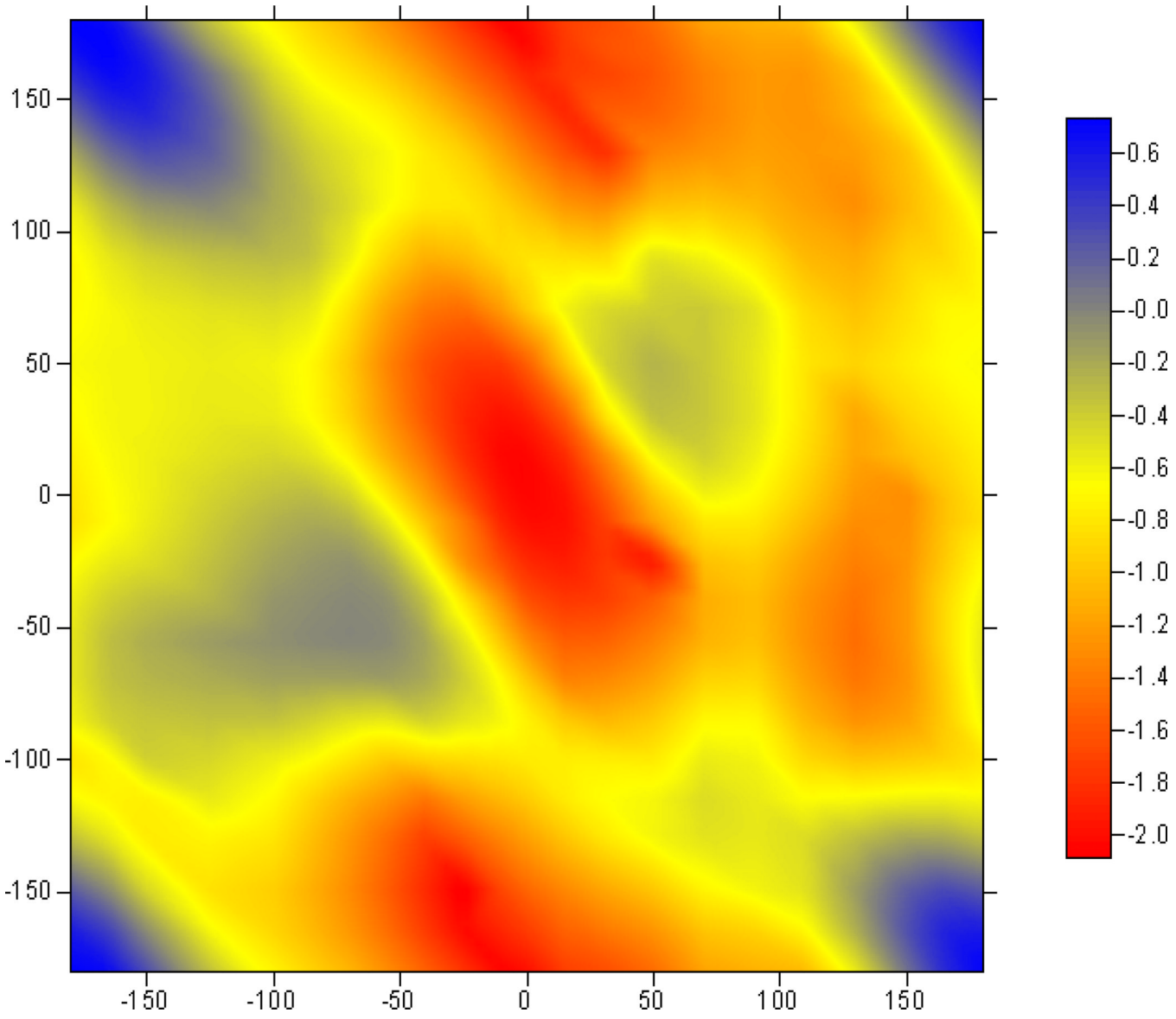

Figure 16.
$^{2}J(C_6\text{-}C_{13})$

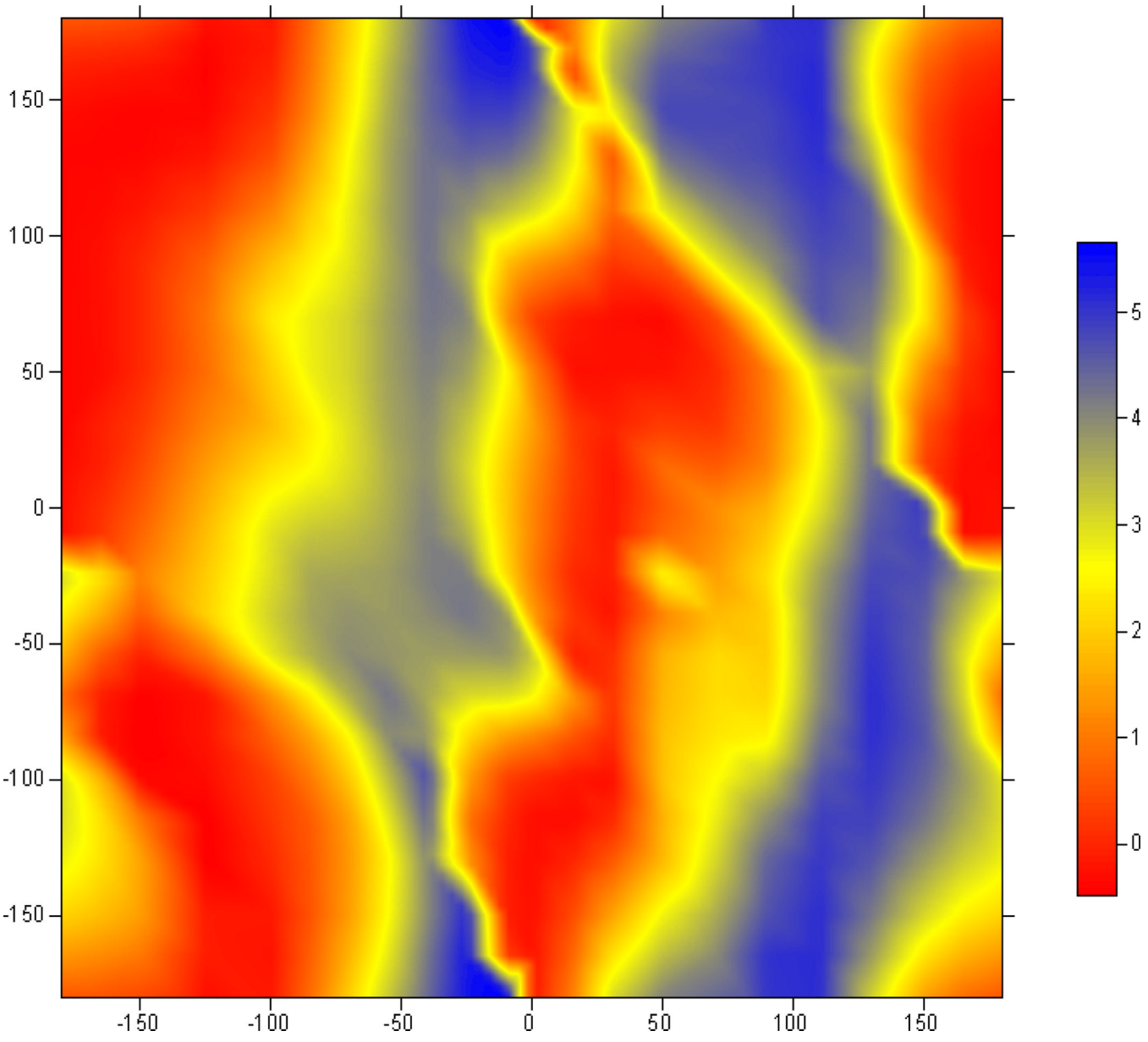

Figure 17.
$^{2}J(H_{12}\text{-}C_{13})$

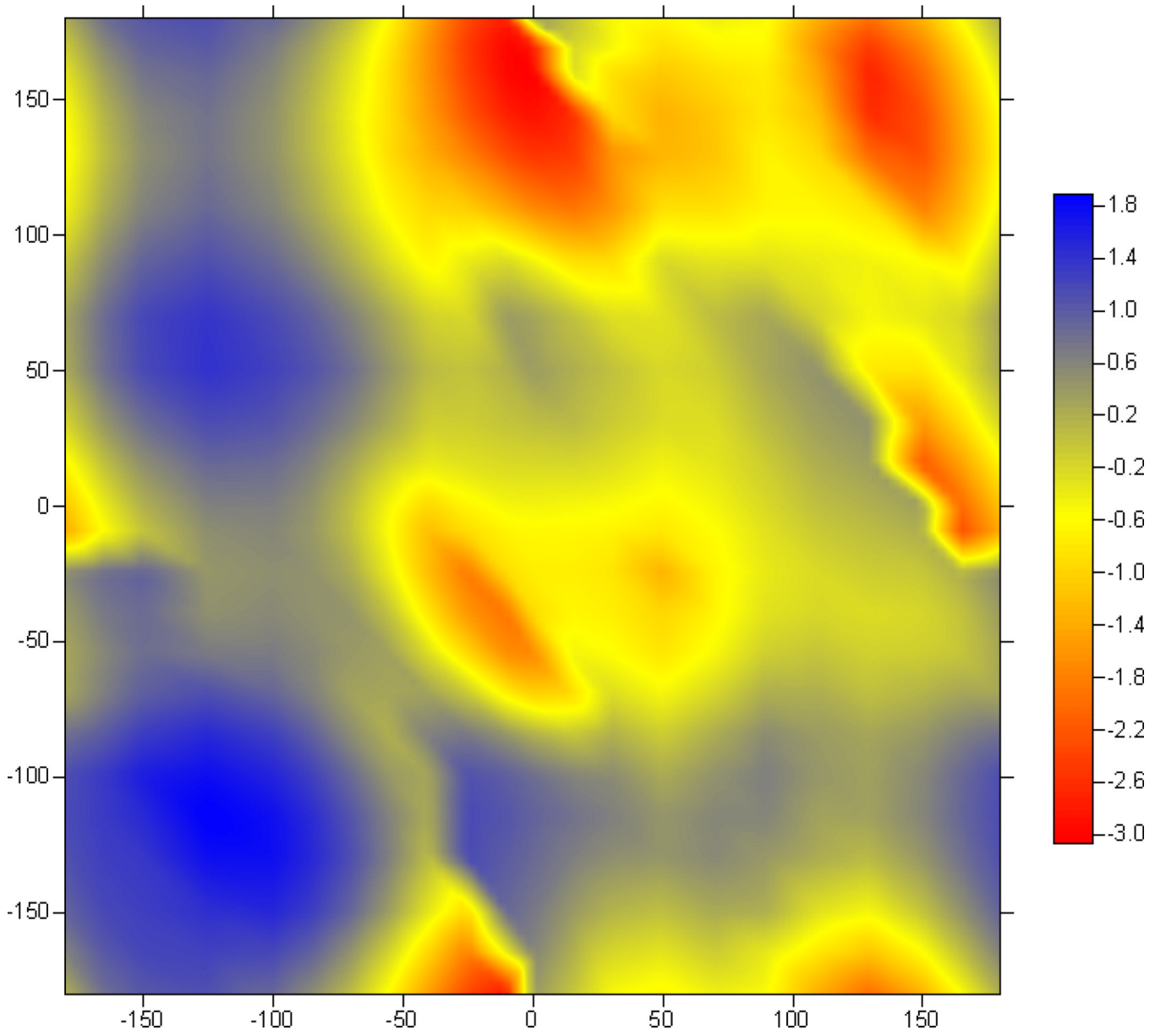

Figure 18.
$^{2}J(N_{11}\text{-}H_{14})$

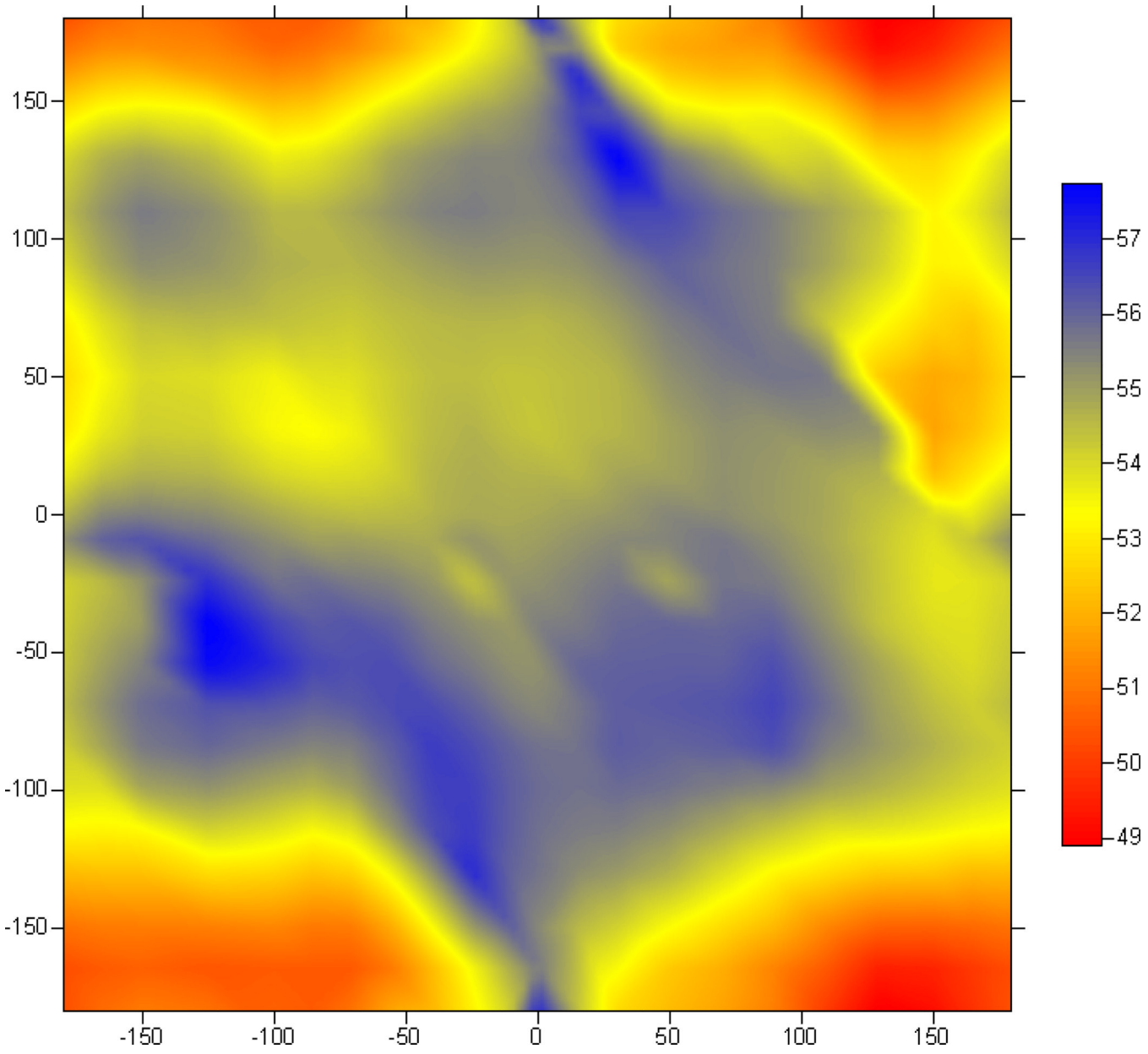

Figure 19.
$^{1}J(C_{13}\text{-}C_{16})$

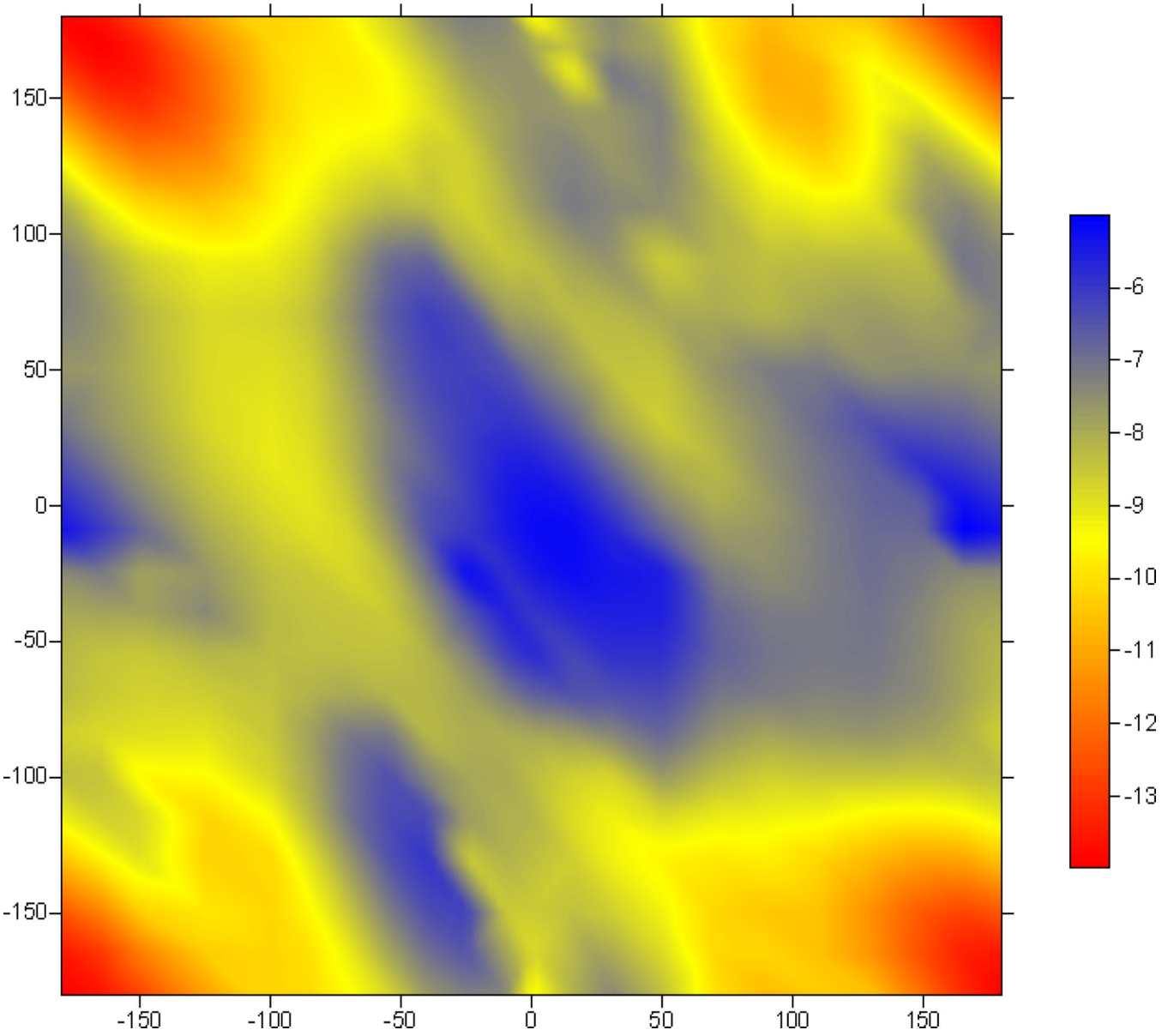

Figure 20.
$^{1}J(N_{11}\text{-}C_{13})$

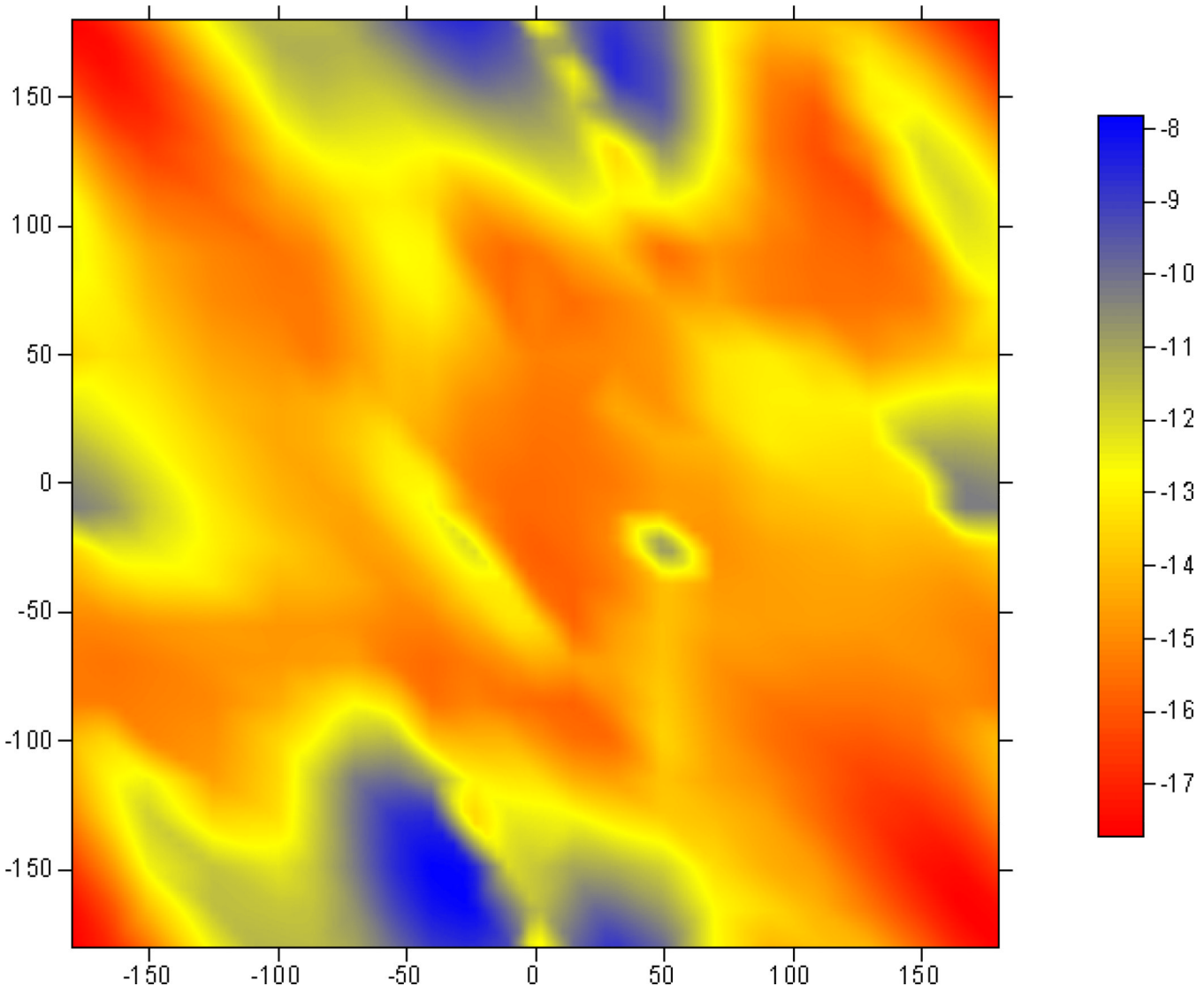

Figure 21.
$^{1}J(C_6\text{-}N_{11})$

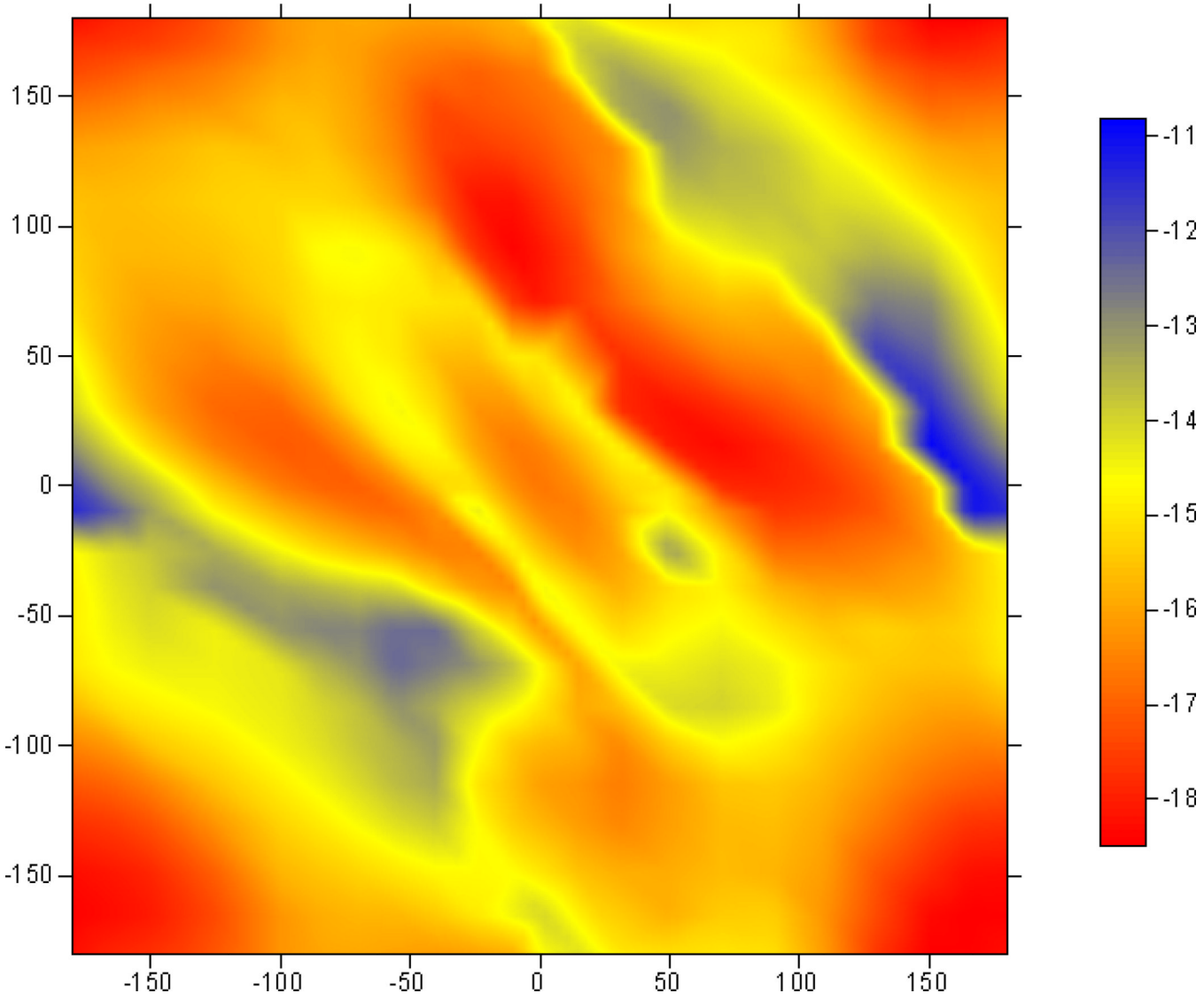

Figure 22.
$^{1}J(C_{16}\text{-}N_{21})$

Table 1

Torsional angles (degrees) of nine representative secondary structures that were completely optimized for comparison with values interpolated from the grid of calculated J's. The regions of the Ramachandran plots in which these dihedrals are found as defined in ref. 34 are indicated.

ϕ	ψ	region
−57	−47	α-helix (right)
−78	59	γ-turn
−57	−70	near α-helix (right)
57	47	α-helix (left)
−49	−26	near α-helix (right)
−139	135	β-sheet
−119	113	β-sheet
−79	150	P_{II}
−51	153	P_{II}

Table 2

Selected J-coupling constants calculated with increasing basis set size (in Hz). Difference (Δ) between values obtained with D95** and cc-pVQZ-su0 basis sets.

J	D95**	cc-pVDZ-su0	cc-pVTZ-su0	cc-pVQZ-su0	Δ
			(−79,150)		
$^{1}J(N_{11},C_{13})$	−9.88	−9.99	−9.54	−9.79	−0.09
$^{2}J(N_{11},C_{16})$	0.60	0.62	0.60	0.61	−0.01
$^{2}J(C_{13},N_{21})$	−11.79	−10.80	−10.76	−11.07	−0.72
$^{3}J(H_{12},H_{14})$	8.74	6.68	9.37	10.44	−1.70
$^{3}J(H_{12},C_{15})$	1.65	1.53	1.52	1.63	0.02
$^{3}J(H_{12},C_{16})$	−0.07	−0.08	−0.10	−0.08	0.01
			(−78,59)		
$^{1}J(N_{11},C_{13})$	−8.18	−8.42	−8.12	−8.36	0.18
$^{2}J(N_{11},C_{16})$	0.19	0.28	0.24	0.23	−0.04
$^{2}J(C_{13},N_{21})$	−9.33	−8.62	−8.51	−8.76	−0.57
$^{3}J(H_{12},H_{14})$	6.21	4.68	6.76	7.67	−1.46
$^{3}J(H_{12},C_{15})$	2.92	2.49	2.73	2.90	0.02
$^{3}J(H_{12},C_{16})$	−0.38	−0.34	−0.35	−0.34	−0.04
			(−119,−113)		
$^{1}J(N_{11},C_{13})$	−10.56	−10.62	−10.19	−10.49	−0.07
$^{2}J(N_{11},C_{16})$	−0.03	0.10	0.04	0.03	−0.06
$^{2}J(C_{13},N_{21})$	−11.30	−10.39	−10.33	−10.64	−0.66
$^{3}J(H_{12},H_{14})$	8.55	6.54	9.00	10.29	−1.74
$^{3}J(H_{12},C_{15})$	0.30	0.20	0.30	0.32	−0.02
$^{3}J(H_{12},C_{16})$	1.07	0.93	0.97	1.01	0.06
			(−49,−26)		
$^{1}J(N_{11},C_{13})$	−7.95	−8.21	−7.93	−8.16	0.21
$^{2}J(N_{11},C_{16})$	0.21	0.28	0.22	0.21	0.00
$^{2}J(C_{13},N_{21})$	−9.29	−8.69	−8.53	−8.76	−0.53

J	D95**	cc-pVDZ-su0	cc-pVTZ-su0	cc-pVQZ-su0	Δ
$^{3}J(H_{12},H_{14})$	2.28	1.57	2.98	3.45	−1.17
$^{3}J(H_{12},C_{15})$	3.91	3.29	3.68	3.89	−0.02
$^{3}J(H_{12},C_{16})$	1.48	1.26	1.58	1.70	−0.22

Table 3

J-coupling constants, mean unsigned error and standard deviation (in Hz) calculated with the midsize (D95**) and large (VQZ') for four representative ideal conformations (See Table 1) of the central residue in acetly-$(Ala)_3$-NH_2 model.

	(−79,150)		**(−78,59)**		**(−119,113)**		**(−49,−26)**			
J	**cc-pVQZ-su0**	**D95****	**cc-pVQZ-su0**	**D95****	**cc-pVQZ-su0**	**D95****	**cc-pVQZ-su0**	**D95****	**MUE**	**σ**
$^{1}J(N_{11},C_{13})$	−9.79	−9.88	−8.36	−8.18	−10.49	−10.56	−8.16	−7.95	0.14	0.16
$^{1}J(C_{13},C_{16})$	50.48	52.53	52.05	53.96	53.01	55.10	53.12	55.40	2.09	0.15
$^{2}J(N_{11},C_{16})$	0.61	0.60	0.23	0.19	0.03	−0.03	0.21	0.21	0.03	0.03
$^{2}J(H_{12},C_{13})$	1.37	1.37	4.04	4.04	3.10	3.19	3.49	3.36	0.06	0.09
$^{2}J(C_{13},N_{21})$	−11.07	−11.79	−8.76	−9.33	−10.64	−11.30	−8.76	−9.29	0.62	0.09
$^{2}J(H_{12},C_{16})$	−2.87	−2.81	−3.62	−3.49	−3.19	−3.21	−5.39	−5.15	0.11	0.11
$^{3}J(C_{6},H_{14})$	1.62	1.62	1.81	1.80	3.13	3.13	0.37	0.30	0.02	0.03
$^{3}J(C_{6},C_{15})$	3.51	3.62	2.93	3.01	1.09	1.11	3.16	3.24	0.07	0.04
$^{3}J(C_{6},C_{16})$	0.36	0.32	0.06	0.03	1.09	1.10	0.48	0.48	0.02	0.02
$^{3}J(H_{12},H_{14})$	10.44	8.74	7.67	6.21	10.29	8.55	3.45	2.28	1.52	0.27
$^{3}J(H_{12},C_{15})$	1.63	1.65	2.90	2.92	0.32	0.30	3.89	3.91	0.02	0.02
$^{3}J(H_{12},C_{16})$	−0.08	−0.07	−0.34	−0.38	1.01	1.07	1.70	1.48	0.08	0.12
$^{3}J(N_{11},N_{21})$	0.02	0.00	−0.19	−0.21	0.06	0.06	−0.42	−0.45	0.02	0.01
$^{3}J(H_{14},N_{21})$	−0.22	−0.26	0.23	0.22	−0.82	−0.89	−1.31	−1.14	0.07	0.11
$^{3}J(C_{15},N_{21})$	−0.03	−0.02	−0.52	−0.53	−0.51	−0.55	0.09	0.12	0.02	0.03
$^{3}J(C_{13},H_{22})$	0.50	0.69	0.06	0.21	0.61	0.79	−0.06	0.04	0.16	0.04

Table 4

Maximum deviation, mean unsigned error (MUE) and standard deviation (σ) of the interpolation errors for selected J couplings from comparison of the completely optimized nine representative structures of table 1 and the values obtained from interpolation of the grid. Atom numbering from figure 1. (see text).

J	Max Dev (Hz)	MUE (Hz)	σ (Hz)
$^{1}J(N_{11},C_{13})$	0.18	0.07	0.06
$^{1}J(C_{13},C_{16})$	0.17	0.05	0.08
$^{2}J(N_{11},C_{16})$	0.04	0.02	0.02
$^{2}J(H_{12},C_{13})$	0.07	0.03	0.04
$^{2}J(C_{13},N_{21})$	0.10	0.03	0.04
$^{2}J(H_{12},C_{16})$	0.04	0.02	0.02
$^{3}J(C_{6},H_{14})$	0.13	0.06	0.08
$^{3}J(C_{6},C_{15})$	0.13	0.06	0.07
$^{3}J(C_{6},C_{16})$	0.08	0.02	0.03
$^{3}J(H_{12},H_{14})$	0.23	0.10	0.12
$^{3}J(H_{12},C_{15})$	0.17	0.06	0.08
$^{3}J(H_{12},C_{16})$	0.29	0.08	0.12
$^{3}J(N_{11},N_{21})$	0.02	0.01	0.01
$^{3}J(H_{14},N_{21})$	0.08	0.02	0.04
$^{3}J(C_{15},N_{21})$	0.03	0.01	0.01
$^{3}J(C_{13},H_{22})$	0.01	0.01	0.00

Table 5

Comparison of J-coupling constants for two low-energy structures of the acetyl-$(Ala)_3$-NH_2 model presenting hydrogen bonds calculated with two basis sets and from interpolation of on the grid.

	C10C10r (−67.3, −10.8)			C10rC7eq (−87.9,−5.1)		
J	**cc-pVQZ-su0**	**D95****	**Grid**	**cc-pVQZ-su0**	**D95****	**Grid**
$^{1}J(N_{11},C_{13})$	−8.33	−8.12	−8.60	−9.47	−9.36	−8.93
$^{1}J(C_{13},C_{16})$	51.97	53.95	55.03	51.83	53.80	54.85
$^{2}J(N_{11},C_{16})$	−0.01	−0.03	−0.09	−0.24	−0.28	−0.90
$^{2}J(H_{12},C_{13})$	3.54	3.44	3.57	3.43	3.40	3.50
$^{2}J(C_{13},N_{21})$	−8.34	−8.84	−9.04	−7.39	−7.83	−8.84
$^{2}J(H_{12},C_{16})$	−5.47	−5.25	−4.98	−5.65	−5.42	−5.09
$^{3}J(C_{6},H_{14})$	1.06	1.07	1.13	2.04	2.07	2.43
$^{3}J(C_{6},C_{15})$	2.99	3.06	3.09	2.35	2.41	2.35
$^{3}J(C_{6},C_{16})$	0.21	0.18	0.11	0.20	0.15	0.18
$^{3}J(H_{12},H_{14})$	6.78	5.29	4.25	10.01	8.30	5.74
$^{3}J(H_{12},C_{15})$	3.26	3.28	3.47	2.12	2.13	3.09
$^{3}J(H_{12},C_{16})$	0.20	0.10	0.34	−0.44	−0.47	−0.12
$^{3}J(N_{11},N_{21})$	−0.39	−0.42	−0.36	−0.30	−0.32	−0.21
$^{3}J(H_{14},N_{21})$	−0.55	−0.43	−0.68	−0.63	−0.50	−0.59
$^{3}J(C_{15},N_{21})$	0.06	0.09	0.10	0.02	0.04	0.09
$^{3}J(C_{13},H_{22})$	0.12	0.22	0.11	0.19	0.28	0.17